Article

The mechanism of mRNA cap recognition

https://doi.org/10.1038/s41586-024-08304-0

Received: 15 November 2023

Accepted: 29 October 2024

Published online: 11 December 2024

Check for updates

Riley C. Gentry[1,5], Nicholas A. Ide[1,5], Victoria M. Comunale[2], Erik W. Hartwick[2,3], Colin D. Kinz-Thompson[2,4] & Ruben L. Gonzalez Jr[2]✉

During translation initiation, mRNA molecules must be identified and activated for loading into a ribosome[1–3]. In this rate-limiting step, the heterotrimeric protein eukaryotic initiation factor eIF4F must recognize and productively interact with the 7-methylguanosine cap at the 5′ end of the mRNA and subsequently activate the message[1–3]. Despite its fundamental, regulatory role in gene expression, the molecular events underlying cap recognition and mRNA activation remain unclear[3]. Here we generate a single-molecule fluorescence imaging system to examine the dynamics with which eIF4F discriminates productive and non-productive locations on full-length, native mRNA molecules. At the single-molecule level, we observe stochastic sampling of eIF4F along the length of the mRNA and identify allosteric communication between the eIF4F subunits that ultimately drive cap-recognition and subsequent activation of the message. Our experiments uncover functions for each subunit of eIF4F and we conclude by presenting a model for mRNA activation that precisely defines the composition of the activated message. This model provides a general framework for understanding how mRNA molecules may be discriminated from one another and how other RNA-binding proteins may control the efficiency of translation initiation.

The different efficiencies with which the ribosome translates individual mRNAs is a tightly regulated, critical component of gene expression. In eukaryotes, much of this regulation is dictated during mRNA activation, whereby mRNA molecules are primed for loading into a ribosomal 43S pre-initiation complex (PIC)[1–3]. More than 95% of cellular mRNAs are activated through a 5′ 7-methylguanosine cap (cap)-dependent process[4,5] driven by the highly conserved eukaryotic initiation factor 4F (eIF4F), a heterotrimeric complex composed of eIF4A, eIF4E and eIF4G[1–3]. Owing to the low abundance of eIF4G and regulated sequestration of eIF4E, mRNA activation is the rate-limiting step of translation for most genes[1,6]. Consequently, healthy cells actively adjust the pool of free eIF4E to drive normal changes in gene expression, while many viruses and diseased cells rely on either physically altered[7] or stoichiometrically dysregulated[8] eIF4F to proliferate.

Despite its prominent role in cellular homeostasis and decades of biochemical research[4–6,9–32], the molecular mechanism by which eIF4F activates mRNAs remains unclear. Previous studies have assigned roles for each component of eIF4F: eIF4E is a small cap-binding protein; eIF4A is a DEAD-box RNA helicase; and eIF4G functions as the core component of eIF4F and a scaffolding protein from which eIF4E and eIF4A exert their activity, while also likely bridging the mRNA to the PIC[1–3]. Using this information, these studies have culminated in a working model for mRNA activation[1–3,33] by which eIF4E functions as the initial point of contact between eIF4F and the mRNA, near the cap in the 5′ untranslated region (UTR) of the mRNA. This contact is then stabilized by the RNA-binding activity of eIF4G. Finally, eIF4A hydrolyses ATP to unwind RNA secondary-structure elements near the cap and results in additional, unknown steps that transition the mRNA from an inactivated state to an activated state.

Notably, there is a plethora of evidence contradicting the model described above[2,3,5,11,15,16,19,21,25,28,30,32–34], and neither the molecular basis for the preferential association between eIF4F and the 5′ UTR of the mRNA, nor the identity of the activated state of the mRNA have been experimentally determined. These questions remain open in part due to the technical limitations of working with eIF4G. Recombinant full-length eIF4G is notoriously difficult to purify and possesses potent non-specific RNA-binding activity[30,35]. Consequently, many biochemical studies have been performed with truncated eIF4G constructs[14,15,19,23,24,26,36–39] together with short, minimal-length mRNA mimics to minimize non-specific binding[15,24,30,38,39]. Biochemical studies have also been hampered by the lack of a complete structure of eIF4F[13,14,27,38]. Moreover, no direct assay for mRNA activation has been developed and, instead, assays that measure ribosome stalling on the start codon, downstream of mRNA activation and subsequent 43S PIC loading are used to indirectly infer eIF4F function[30,35].

To overcome these limitations and determine the mechanism of mRNA activation, here we developed a single-molecule fluorescence resonance energy transfer (smFRET) system that probes the binding of yeast eIF4F to local segments of a native, full-length mRNA. To achieve this, we site-specifically labelled native mRNAs at either cap-proximal or cap-distal locations, and site-specifically labelled full-length eIF4G, enabling us to systematically investigate the binding kinetics of eIF4F and eIF4F subcomplexes at cap-proximal and cap-distal locations on full-length mRNA. By comparing the rates determined by our experiments, which span >60,000 individual molecules queried across >80 experimental conditions, we identify the molecular basis for cap recognition and ascribe functions to each subunit of eIF4F. By directly following eIF4G, we isolate an intermediate in mRNA activation and

[1]Department of Biological Sciences, Columbia University, New York, NY, USA. [2]Department of Chemistry, Columbia University, New York, NY, USA. [3]Present address: BioChemistry Krios Electron Microscopy Facility, Department of Biochemistry, University of Colorado Boulder, Boulder, CO, USA. [4]Present address: Department of Chemistry, Rutgers University-Newark, Newark, NJ, USA. [5]These authors contributed equally: Riley C. Gentry, Nicholas A. Ide. ✉e-mail: rlg2118@columbia.edu

define the activated state of the mRNA. These insights enable us to conclude by presenting a model for mRNA activation, which implies new ways in which cells probably regulate gene expression.

Observing dynamic eIF4G–mRNA binding

To develop a system enabling us to monitor mRNA binding by eIF4F and eIF4F subcomplexes, we first reconstituted *Saccharomyces cerevisiae* translation initiation according to established protocols[30,35,40,41] (Extended Data Fig. 1a). Notably, we optimized the purification procedure for eIF4G, enabling us to purify large quantities of full-length eIF4G almost entirely free of degradation products, which are otherwise common contaminants in eIF4G preparations[30,35]. We validated the function of recombinant eIF4F using a standard native gel-shift assays with a capped *S. cerevisiae* mRNA encoding the gene *rpl41a*[30,35]. This assay measures the ability of 43S PICs to load onto and scan to the start codon of capped mRNAs. As expected, efficient ribosome recruitment was dependent on eIF4F, with reactions lacking eIF4E but containing eIF4G and eIF4A showing diminished but detectable recruitment[30] (Extended Data Fig. 1b). We next performed titration-regime ensemble binding measurements using fluorescence anisotropy to measure the binding behaviour of eIF4G with a short, uncapped 51-nucleotide fragment of *rpl41a* containing the 5′ UTR and first 9 codons[42]. Consistent with previous publications, we observed that eIF4G associated tightly[30] and multivalently[5] with the short, uncapped mRNA fragment (Extended Data Fig. 1c).

To assess the validity of a model in which eIF4E functions as the first point of contact between eIF4F and the mRNA 5′ UTR, one must compare the binding behaviour of eIF4F at cap-proximal and cap-distal locations in the absence and presence of the cap and eIF4E. The robust, non-specific RNA-binding activity of eIF4G complicates measurement of eIF4F association with the cap because most assays are agnostic to binding location. We therefore sought to develop an assay sensitive to the binding location of eIF4F on full-length mRNAs using a series of smFRET constructs to probe the association and dissociation kinetics of both eIF4F and eIF4F-subcomplexes to cap-proximal and cap-distal locations on full-length *rpl41a*. We site-specifically labelled *rpl41a* using a deoxyribozyme[43] and selectively capped the labelled mRNAs to generate three constructs: (1) capped *rpl41a* with a cap-proximal Cy3 FRET donor fluorophore located at nucleotide 14 on the mRNA (capped); (2) uncapped *rpl41a* with a cap-proximal Cy3 (uncapped); and (3) capped *rpl41a* with a cap-distal Cy3 located at position 92 on the mRNA (cap-distal) (Fig. 1a). Next, we site-specifically labelled eIF4G with the Cy5 FRET acceptor fluorophore at the linker region between the eIF4E-binding motif and the second RNA-binding motif (Extended Data Fig. 1a). The Cy3- and Cy5-labelled mRNA and protein pairs enable us to directly observe the binding kinetics of any Cy5–eIF4G-containing complex to localized cap-proximal or cap-distal positions on full-length Cy3–*rpl41a* mRNA (Cy3–*rpl41a*).

We performed our experiments using a wide-field, prism-based, total internal reflection fluorescence microscope, which enables the collection of videos containing information from hundreds of individual molecules simultaneously (Supplementary Video 1). To perform these single-molecule experiments, we sparsely tether individual Cy3–*rpl41a* mRNAs hybridized at an internal position in the mRNA with a short biotinylated DNA-oligonucleotide to the surface of a quartz flowcell passivated with a mixture of methoxy-terminated polyethylene glycol (PEG) and biotin-terminated PEG through a biotin–Streptavidin bridge (Fig. 1b). We can inject and freely exchange solution in the flowcell before and during experiments, enabling both steady-state and pre-steady-state measurements. After tethering the Cy3–*rpl41a* mRNA, we inject Cy5–eIF4G-containing complexes into the flowcell, and directly excite Cy3 with a total internal reflection laser light. When Cy5–eIF4G binds to the mRNA at a position within around 7 nm of the Cy3 on the Cy3–*rpl41a*, FRET causes the Cy3 emission to decrease while stimulating Cy5 emission (Extended Data Fig. 2a,b). Although the real power of single-molecule experiments comes from the analysis of individual trajectories, many of the conclusions in this work can be surmised by viewing the unprocessed videos (Supplementary Videos 1–7).

Before performing experiments on full-length *rpl41a* mRNA, we first validated our choice of labelling constructs by performing smFRET experiments between the covalently labelled Cy5–eIF4G co-purified as a complex with eIF4E (hereafter Cy5–eIF4G:E), and the capped, 24-nucleotide 5′ UTR of *rpl41a* with the cap-proximal Cy3 labelling position, which we expected to bind to only a single eIF4G molecule (Extended Data Fig. 2a,b). These experiments confirm robust FRET between the Cy3–mRNA fragment and Cy5–eIF4G:E and reveal a rapid but transient association of Cy5–eIF4G:E with the 5′ UTR (Supplementary Video 1 and Extended Data Fig. 2c). Notably, both the association and dissociation rates of eIF4G:E scaled with increasing concentration (Extended Data Fig. 2d,e). Concentration-dependent dissociation rates are indicative of facilitated dissociation—a phenomenon that has been observed for multiple nucleic-acid-binding proteins that make multivalent interactions with their substrates[44–48]. As eIF4G possesses three RNA-binding motifs, at any given time, one or more of these motifs may dissociate from the mRNA while the others remain bound, therefore preventing eIF4G from being released from the mRNA. However, when an individual binding motif releases from the mRNA, the vacancy can be filled by another competing eIF4G molecule, which in turn facilitates the dissociation of the original eIF4G molecule (Extended Data Fig. 2f). To confirm this phenomenon, we allowed Cy5–eIF4G:E to associate with the 24-nucleotide 5′ UTR of *rpl41a* and injected unlabelled eIF4G:E into the flowcell at increasing concentrations and observed the concentration-dependent replacement exchange of the fluorophore-labelled eIF4G:E with unlabelled eIF4G:E (Extended Data Fig. 2g). Owing to facilitated dissociation, off events measured at steady-state can represent stochastic dissociation, facilitated exchange with another molecule or conformational fluctuations that happen during those exchange events. This leads to multiphasic steady-state off rates, which we fit to bi-exponential functions. Throughout this Article, we report the population-weighted average of the two phases to contrast the pre-steady-state stochastic dissociation events from the convoluted steady-state exchange events (Extended Data Fig. 3a), but all population weights are provided in Supplementary Table 1.

eIF4G binds tightly and non-specifically

Having validated the smFRET constructs, we sought to understand the molecular basis for 5′ end recognition by eIF4F. As eIF4G provides most of eIF4F's binding stability to mRNA and eIF4E directly associates with the cap[5,16,20,25,30], we hypothesized that we could determine the basis for the assumed preferential association of eIF4F with the mRNA 5′ end by measuring the association and dissociation rates of Cy5–eIF4G and Cy5–eIF4G:E to the capped, uncapped and cap-distal constructs (Fig. 1a; cases in which identical experiments containing either Cy5–eIF4G or Cy5–eIF4G:E were performed are hereafter denoted Cy5–eIF4G/eIF4G:E). To determine association (k_{on}) and dissociation (k_{off}) rate constants, we performed pre-steady-state measurements. To measure association rates, we delivered Cy5–eIF4G/eIF4G:E to surface-tethered Cy3–*rpl41a* while initiating data collection (Fig. 1b (injection) and Supplementary Videos 2 and 3). The waiting time between the delivery of Cy5–eIF4G or Cy5–eIF4G:E and the first binding event is indicative of the association rate in pre-steady-state conditions, while the apparent association and dissociation rates in steady state can be inferred from the later timepoints for each individual molecule (Fig. 1c). Notably, we observed that eIF4G:E facilitates its own dissociation on the full-length constructs as well, convoluting the steady-state data (Extended Data Fig. 3a–c). Thus, to measure dissociation rates, we performed pre-steady-state experiments in which we started with Cy3–mRNA molecules pre-bound

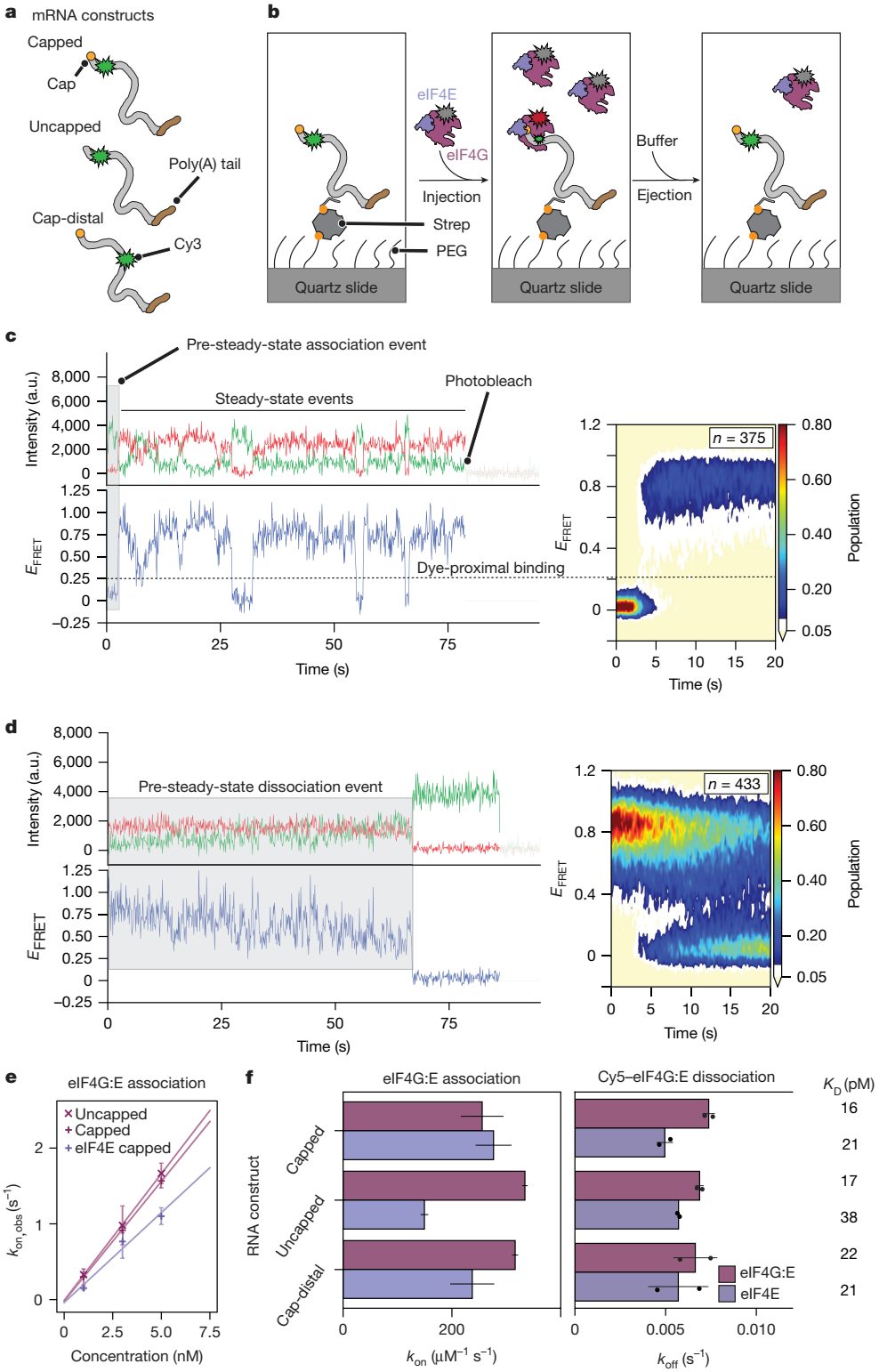

Fig. 1 | eIF4G/eIF4G:E stably associates with mRNA independent of is binding position or the cap. a, Schematic of the full-length, Cy3-labelled *rpl41a* mRNA constructs used in this study. **b**, Schematic of the stopped flow injection and ejection pre-steady-state experiments used to measure k_{on} and k_{off}. **c**, An example trace taken from a Cy5–eIF4G:E injection experiment is shown. The trace can be divided into two portions: the first binding event in the trajectory encompasses the pre-steady-state portion, whereas the later portions of the trajectory display steady-state binding and dissociation events until bleaching of the donor fluorophore. Right, a surface contour plot showing the aggregate behaviour of all of the trajectories in an injection experiment. a.u., arbitrary unit. **d**, The equivalent example trace and surface contour plot for Cy5–eIF4G:E ejection experiments are shown. As all of the excess Cy5–eIF4G:E has been removed from the flowcell, only the pre-steady-state behaviour can be inferred from ejection experiments. **e**, The association rate of Cy5–eIF4G/eIF4G:E is linear with respect to concentration and depends more on the presence of eIF4E than on the cap. $n = 2$ biological experiments for every condition. **f**, Quantification of the pre-steady state association and dissociation rates for Cy5–eIF4G/eIF4G:E, demonstrating that eIF4G uniformly binds to mRNA irrespective of the cap or its binding location. $n = 2$ experiments for every condition. For **e** and **f** (right), data are mean ± s.d. For the association rate bar plot in **f** (left), the bar coordinate corresponds to the fit shown in **e** and the error is the error of the fit.

to Cy5–eIF4G/eIF4G:E, and then removed all free protein by flushing the flowcell with buffer lacking initiation factors (Fig. 1b (ejection)) and measured the time required for Cy5–eIF4G/eIF4G:E dissociation (Fig. 1d). Cy5–eIF4G/eIF4G:E binding to the mRNA resulted in a broad distribution of FRET efficiencies (E_{FRET}), probably due to eIF4G binding at slightly different positions along the mRNA (Fig. 1c,d (right)). Thus, to prevent overinterpretation of the different E_{FRET} values, we simplified our analysis to classify E_{FRET} states only as either bound or unbound, corresponding to high and low (near zero) E_{FRET} values (Fig. 1c,d).

We measured the association rates between Cy5–eIF4G/eIF4G:E and each mRNA construct. If cap recognition by eIF4E serves as the initial point of contact between eIF4F and the mRNA, one would predict that Cy5–eIF4G:E would most rapidly associate to cap-proximal positions, while association of Cy5–eIF4G in the absence of eIF4E would not be expected to display any cap dependence. Notably, eIF4G associated rapidly with the mRNA in all of the experiments, with association rate constants ranging from 150 to 300 $\mu M^{-1} s^{-1}$, which was independent of the cap and the binding position of eIF4G (Fig. 1e). We observed a slight decrease in the association of Cy5–eIF4G to cap-proximal positions in the absence of eIF4E, but this effect was not cap dependent (Fig. 1e). These measurements show that any additional interaction between eIF4E and the cap does not allow eIF4G:E to more rapidly associate with cap-proximal positions on mRNA.

Having observed little variation in the association rates of eIF4G, we expected eIF4E to selectively stabilize eIF4G:E at the cap. Notably, eIF4G dissociated very slowly from all three mRNA constructs both with and without eIF4E (Fig. 1f and Extended Data Fig. 3). Our initial experiments measured dissociation rates slow enough that they were limited by photobleaching, so we performed experiments in which we shuttered the excitation laser every 3 s to better preserve the fluorophores and, under these conditions, Cy5–eIF4G and Cy5–eIF4G:E remained bound for upwards of minutes (Fig. 1f). Notably, we also performed an experiment with 30 s shuttering intervals and this experiment showed stable eIF4G:E association for tens of minutes (Supplementary Video 4); thus, the k_{off} values that we observed (Fig. 1f) probably represent the upper bounds for the true dissociation rate of eIF4G from the mRNA. These dissociation rates may also not necessarily reflect true dissociation rates from the mRNA molecule because facilitated dissociation may allow for intra-mRNA hopping[46], whereby a microdissociated RNA-binding domain of eIF4G may bind to another segment on the same RNA and facilitate the movement of eIF4G along the mRNA (Extended Data Fig. 4). These hopping events manifest as a recovery of E_{FRET} after dissociation of eIF4G from the fluorophore-proximal location. On the capped 24-nucleotide UTR of *rpl41a* that contains only a single eIF4G:E-binding site, recovery of E_{FRET} occurs only around 5% of the time (Extended Data Fig. 4), which may be due to conformational fluctuations of eIF4G:E or the mRNA or to photoblinking of the Cy5 fluorophore. By contrast, on full-length *rpl41a*, hopping events can be observed in around 25% of our trajectories under constant illumination. In conditions in which we preserve the fluorophore by shuttering the laser, this increases to about 45%, although it also allows for the possibility of transient events being missed during the time the laser is shuttered off. In both cases, detection of a bona fide hopping event requires two observations—dissociation of eIF4G from the fluorophore-proximal location and recovery of E_{FRET} when the same eIF4G, or another eIF4G bound elsewhere on the mRNA, hops back to a fluorophore-proximal position. The stringency of these requirements, combined with the short lifetimes of our fluorophores, probably lead to a systematic under-representation of how often hopping events occur.

Although upper bounds, the k_{off} values that we measured are still informative because they provide upper limits for the equilibrium dissociation constants (K_D) of eIF4G/eIF4G:E in the range of 10–50 pM for each mRNA construct (Fig. 1f). To eliminate the possibility that our cap-proximal and cap-distal fluorophores were reporting on the same, cap-proximal binding location due to mRNA structure, we generated a short, 47-nucleotide, RNA fragment approximately 20 nucleotides upstream and downstream of the cap-distal fluorophore and observed binding between Cy5–eIF4G:E and this isolated fragment (Extended Data Fig. 3d,e). Consistent with the cap-distal fluorophore reporting on a distinct location, eIF4G:E tightly and rapidly associated with this isolated, uncapped internal fragment similarly to how it bound the cap-distal location in the context of the full-length, capped mRNA. Furthermore, we also tested binding to a second cap-distal fluorophore position on an uncapped mRNA approximately 100 nucleotides downstream of the first location, achieving the same result (Extended Data Fig. 3d,e).

Having established that our constructs report on distinct binding locations, variations in the affinity of eIF4G/eIF4G:E across productive, capped, locations on the mRNA and non-productive, uncapped and cap-distal positions, are minor. These minor differences cannot be reconciled with a model for mRNA activation that begins with preferential association of eIF4F at the 5′ cap. The lack of cap dependence suggests that the functional consequence of cap recognition may occur at a step downstream of initial binding by eIF4G:E[5]. However, the cellular concentration of eIF4G is roughly stoichiometric to that of mRNA molecules[6], and each molecule contains multiple potential non-specific binding sites. As eIF4G dissociates so slowly from these cap-distal, non-productive locations on the mRNA, it is unlikely that eIF4G:E simply passively samples the mRNA and only selectively functions when bound to cap. Although eIF4G can be stably co-purified with eIF4E[18,30,35], another possibility is that eIF4E dissociates from RNA-bound eIF4G unless the cap is nearby to provide additional stability; the absence or presence of eIF4E may therefore distinguish productive and non-productive eIF4G.

eIF4G:E lacks cap specificity

As we placed the acceptor fluorophore on eIF4G, we were not able to distinguish whether eIF4E was present when eIF4G bound to the mRNA. To ascertain whether eIF4E was present when eIF4G:E was bound to each of the capped, uncapped and cap-distal mRNA constructs, we used a site-specifically Cy5-labelled eIF4E (Cy5–eIF4E) that has been characterized[16,20,25]. Consistent with the literature[16,20,25], Cy5–eIF4E showed very transient sampling of the cap (Fig. 2a and Supplementary Video 5 (left)), and did not show detectable binding to the uncapped or cap-distal constructs. Similar to Cy5–eIF4G:E, when we used eIF4G:E–Cy5, generated by supplying unlabelled eIF4G to Cy5–eIF4E, the steady-state time between association events was reduced and the duration of binding events was lengthened by nearly an order of magnitude[16,20,25] (Fig. 2b and Supplementary Video 5 (right)) but the complex still facilitated its own dissociation (Extended Data Fig. 5). Unexpectedly, but in agreement with our Cy5–eIF4G:E experiments, eIF4G:E–Cy5 showed no cap or positional dependence on association or dissociation in either steady-state (Fig. 2b) or pre-steady state measurements (Fig. 2c and Supplementary Video 6). The eIF4G:E association and dissociation rates for experiments using Cy5–eIF4E matched those measured in experiments using Cy5–eIF4G (Fig. 2c), demonstrating that eIF4G and eIF4E function in concert as a complex, even when bound to cap-distal locations on mRNA. The lack of cap specificity suggests that, rather than serving as the initial point of contact between eIF4F and the mRNA, cap sensing by eIF4E is probably functionally relevant downstream of the initial binding event. However, if the cap does not function as a scaffold to assemble eIF4F at the correct location on the mRNA as previously thought[1–3], some other factor must direct eIF4F binding to the 5′ end.

eIF4A drives cap recognition

To examine the role of the 5′ cap during mRNA activation, we focused on eIF4A and eIF4B, which are thought to participate in mRNA activation downstream of eIF4F binding[1–3]. Using Cy5–eIF4G, we assessed the binding behaviour of Cy5–eIF4G:E to each of the mRNA

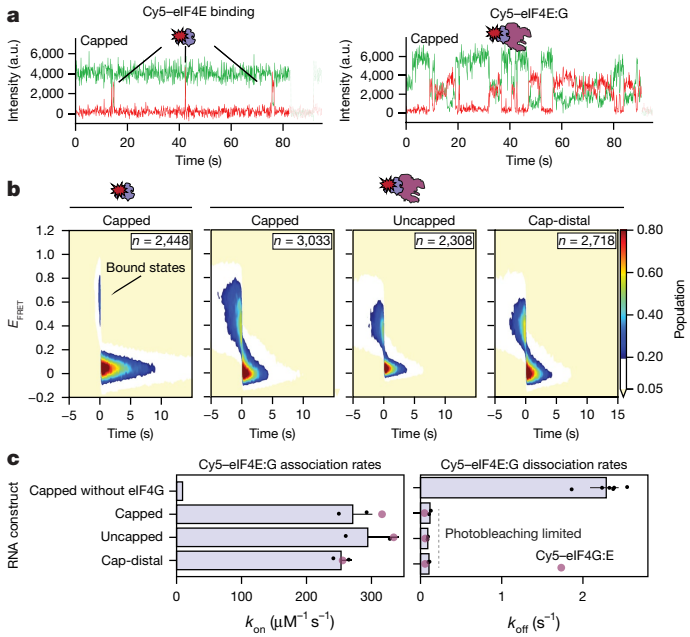

Fig. 2 | eIF4E functions in concert with eIF4G irrespective of the cap. **a**, Example trajectories of Cy5–eIF4E binding to the capped mRNA construct in the absence (left) or presence (right) of unlabelled eIF4G. In the absence of eIF4G, Cy5–eIF4E only transiently samples the cap, whereas it stably binds in the presence of eIF4G. **b**, Surface contour plots post-synchronized to the steady-state transitions of eIF4E out of the bound state. Time = 0 marks the time at which eIF4E dissociates from the vicinity of the donor fluorophore, such that the negative time axis indicates how long Cy5–eIF4E remains bound before dissociation and the positive time axis shows the delay time between binding events. **c**, Quantification of the association and dissociation rates of Cy5–eIF4E and eIF4G:E–Cy5 from the three mRNA constructs. The association rates for the capped, uncapped and cap-distal constructs were determined from experiments performed at 5 nM eIF4G:E–Cy5, whereas the eIF4G-capped association rate was derived from the slope of the apparent association rates of Cy5–eIF4E performed across three concentrations. The nearly identical rates derived from equivalent experiments performed with Cy5–eIF4G, plotted in Fig. 1, are shown as purple dots to aid the comparison between Cy5–eIF4E and Cy5–eIF4G. $n = 2$ biological experiments for each experimental condition. As the eIF4G-capped rates were determined using a concentration series and this condition does not facilitate its own dissociation, the dataset for each concentration point was used to calculate the dissociation rate ($n = 6$). Data are mean ± s.d., except for the eIF4G-capped association rate, for which the value was calculated from the fit of the association rate concentration series and the error bar corresponds to the error of the fit.

constructs in the presence of eIF4A, eIF4B and ATP·Mg^{2+}. We began with tethered Cy3–mRNA constructs and delivered small amounts of Cy5–eIF4G:E in the presence of saturating amounts of eIF4A and ATP·Mg^{2+} (Cy5–eIF4G:E + eIF4A) or eIF4A, eIF4B and ATP·Mg^{2+} (Cy5–eIF4G:E + eIF4A + eIF4B) and measured the waiting time for the first binding event. Similar to Cy5–eIF4G:E, Cy5–eIF4G:E:A:B showed neither a cap nor positional dependence on its association with mRNA in the steady-state or pre-steady-state contexts (Extended Data Fig. 6a,b). However, the steady-state experiments in the presence of eIF4A and eIF4A + eIF4B showed cap-dependent changes in the dissociation behaviour (Extended Data Fig. 6b). As eIF4A is able to associate with mRNA in the absence of eIF4G, we tested whether eIF4A-bound mRNAs would behave differently by pre-equilibrating the capped and uncapped constructs with eIF4A and then repeated the injection of Cy5–eIF4G:E + eIF4A; only a modest (around twofold) decrease in association was observed (Extended Data Fig. 6e,f).

To better assess the effects of eIF4A, eIF4B and ATP·Mg^{2+} on the dissociation rate of Cy5–eIF4G:E, we performed pre-steady-state experiments. In these experiments, we began with Cy5–eIF4G:E bound to the mRNA, and exchanged the buffer with new buffer containing saturating amounts of eIF4A, eIF4B and ATP·Mg^{2+}, but lacking eIF4G and eIF4E (Fig. 3 (right)). We compared these experiments to the dissociation experiments performed earlier (Fig. 3 (left)), in which we delivered buffer containing no additional proteins. We performed two sets of experiments: one in which the laser continuously illuminated the sample, and one in which the laser was shuttered every 3 s, enabling us to determine the rates at both the second and minute timescale (Fig. 3a–d).

We observed that Cy5–eIF4G/eIF4G:E remains stably associated for minutes with all mRNA constructs in the absence of eIF4A, eIF4B and ATP (Fig. 3a–e). However, contrary to all expectations, in the presence of eIF4A, eIF4B and ATP, binding of Cy5–eIF4G/eIF4G:E to the mRNA was destabilized by around 30–40-fold under all of the conditions tested in which cap recognition was not possible (Fig. 3b–e and Extended Data Fig. 7a–c). This 30-fold destabilization requires ATP binding, but both eIF4B and ATP hydrolysis are dispensable for stripping (Extended Data Fig. 7c–g). By contrast, under the single condition in which cap recognition was possible, Cy5–eIF4G:E was around tenfold stabilized relative to the other conditions. This order-of-magnitude increase in stability demonstrates that eIF4A discriminates the productive association of Cy5–eIF4G:E at the cap from non-productive association at cap-distal positions (Fig. 3e and Supplementary Video 7). To assess whether eIF4A needs to directly interact with eIF4G, we titrated the amount of eIF4A used in the stripping experiments (Extended Data Fig. 8a,b). Similar to its effect on the observed rate on in vitro mRNA recruitment, the strippase activity of eIF4A was half-maximal between 100–200 nM eIF4A and saturated at around 1 μM. This correlates well with the affinity of eIF4A for eIF4G:E[30], but is substantially below its affinity for RNA, which we measured to be around 10 μM for the 5′ UTR of *rpl41a* (Extended Data Fig. 8c), leading us to conclude that this strippase activity is a consequence of direct eIF4G:A interaction. From these experiments, we conclude that eIF4A is a strippase that removes eIF4G/eIF4G:E from non-productive locations. Moreover, we observed that cap recognition by eIF4E inhibits this strippase activity, probably through allosteric changes in eIF4G, as eIF4E and eIF4A do not directly interact. More broadly, our experiments illustrate that cap recognition is a multistep process during which eIF4F must stochastically sample many binding locations and be recycled by eIF4A before arriving at the cap. Thus, the transient, but relatively long-lived eIF4F-binding event at the cap is the 'activated state' of the mRNA. This cap-dependent stalling of eIF4F then probably functions as a beacon that facilitates the downstream loading of the PIC onto the 5′ end of the mRNA through a bridge between eIF4G and eIF3 or eIF5[10]. Consistent with this model, 48S PIC formation is abolished in the absence of eIF4A, and perturbation of cap recognition by either removal of eIF4E or its mutation to weaken cap-binding confers an approximately tenfold rate defect that can be compensated for by increasing the concentration of eIF4G, and therefore increasing the time that it spends at the cap despite its active removal (Extended Data Fig. 8d). This conclusion is further supported by recent single-molecule observations demonstrating that pre-incubating mRNA with eIF4F before 43S PICs removes the slow step of mRNA loading in a manner dependent on the concentration of eIF4A[49].

We were interested in whether eIF4A might function by stepwise stripping of eIF4E from eIF4G and then eIF4G from the mRNA, so we performed similar experiments with eIF4G:E–Cy5, but the dissociation rates were within twofold of those with Cy5–eIF4G:E (Extended Data Table 1), suggesting that eIF4G:E is ejected as a complex (Extended Data Fig. 5 shows all Cy5–eIF4E experiments).

Discussion

How eIF4F activates mRNA for translation has remained unclear since its discovery. Current models for mRNA activation begin with

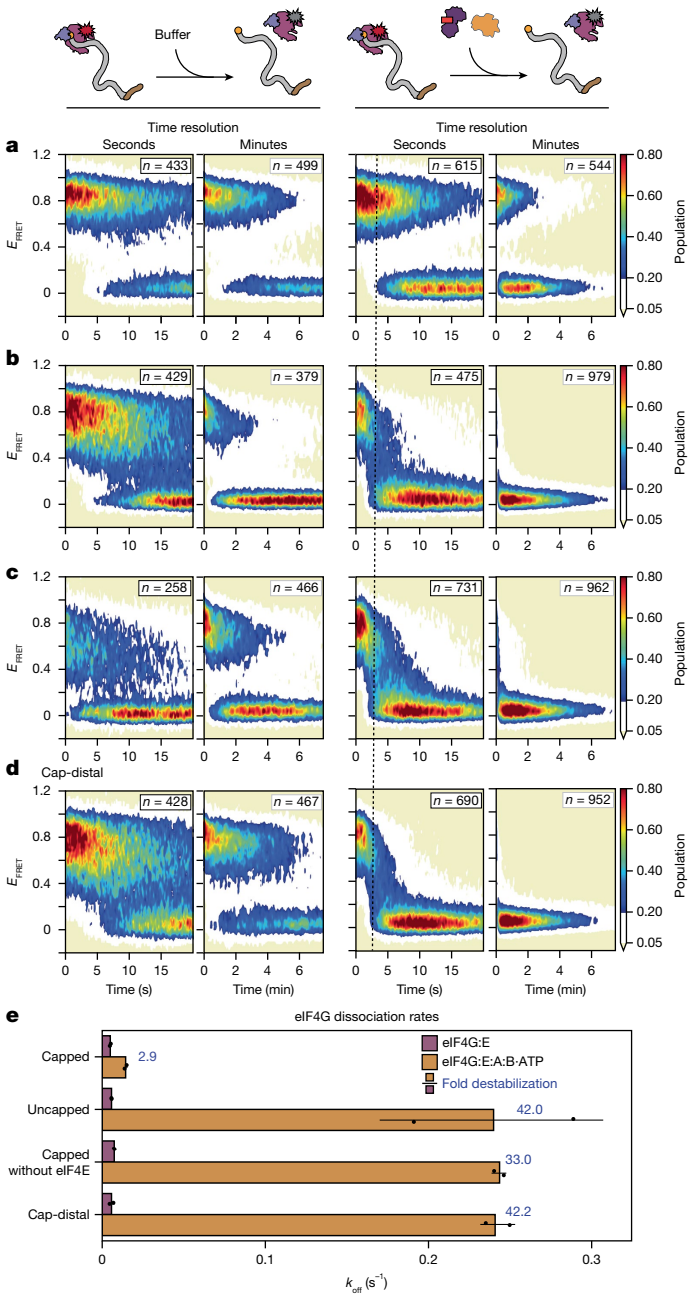

Fig. 3 | eIF4A strips eIF4G:E from RNA. a–**d**, Surface contour plots showing ejection experiments in which excess, unbound Cy5–eIF4G:E in the flowcell is replaced with buffer lacking Cy5–eIF4G:E or replaced with buffer lacking Cy5–eIF4G:E but supplemented with eIF4A, eIF4B and ATP (right). Each experiment was recorded at both 10 fps and 1/3 fps to obtain kinetic information at both the second and minute timescales. These experiments were performed on the capped RNA (**a**) and uncapped RNA (**b**), and capped RNA without eIF4E (**c**), and internal mRNA constructs (**d**). Each experiment begins with Cy5–eIF4G:E bound to the RNA. E_{FRET} starts at a high value and remains stable until photobleaching in the absence of eIF4A, eIF4B and ATP. However, in the presence of eIF4A, eIF4B and ATP, E_{FRET} rapidly decays within around 3 s (guiding line). This indicates that eIF4A strips eIF4G:E from the RNA. eIF4E recognition of the cap (**a**) is able to resist this stripping. **e**, Pre-steady-state off rates were calculated from the individual trajectories of the experiments performed in **a**–**d**. These rates show that eIF4G is destabilized by 30–40-fold in the presence of eIF4A, eIF4B and ATP, but eIF4G is resistant to this destabilization in the presence of both eIF4E and the cap. $n = 2$ biological experiments for each experimental condition. Data are mean ± s.d.

the preferential association of eIF4F with the cap-proximal 5′ UTR of the mRNA, guided by an initial contact of eIF4E with the cap[1–3,16,25]. Afterwards, eIF4F hydrolyses ATP to exert an unknown activity that transforms the mRNA into a compositionally undefined activated state through a series of steps that are unclear[1–3], after which some studies have suggested eIF4A recycles the complex[4,16,29,34].

Contrary to expectations, our single-molecule experiments (summarized in Extended Data Table 2) define a molecular mechanism whereby eIF4E does not initially bind to the cap, but instead acts together with eIF4G and eIF4A to find the 5′ cap, therefore forming the activated state. Notably, we found that eIF4G:E tightly and non-specifically binds to locations throughout an mRNA regardless of the cap, and rather than functioning solely as a helicase, eIF4A instead strips eIF4G:E from uncapped and cap-distal positions. Although unexpected, this result is consistent with the requirement for eIF4A regardless of whether or not there is the cap-proximal secondary structure in the mRNA[11,22] and is also consistent with some early speculations about the enzyme[33]. Moreover, we found that, rather than functioning as the initial point of binding for eIF4F complex assembly, eIF4E recognition of the cap occurred downstream of the initial eIF4G:E-binding event[5]. Cap-recognition by eIF4E allosterically inhibited eIF4A through eIF4G, preventing it from stripping eIF4G:E, therefore forming the activated state of the mRNA. Although the helicase activity of eIF4A is modestly stimulated by eIF4G:E, it is still a poor RNA helicase[11,19,50]. Furthermore, as eIF4A is essential for mRNA recruitment even on unstructured mRNAs[11,22,51], which probably do not require a helicase, we speculate that, in addition to its helicase activity, a primary function of eIF4A as part of eIF4F during mRNA activation is that of an ATP-dependent strippase. As other DEAD-box proteins have been shown to displace proteins from RNA[52], we cannot exclude the possibility these proteins (such as ded1, dbp1[22,51,53,54]) share activities that are redundant with those of the essential eIF4F subunit eIF4A. Moreover, our observation that eIF4A functions in a capacity other than as an RNA helicase is consistent other non-helicase functions that have been identified for eIF4A in the human translation system[17,21]. Notably, as eIF4A is present at such a high cellular concentration[6], a considerable amount of free eIF4A is expected to be present in the cell. Such excess free eIF4A has been suggested to participate in translation by binding to mRNA[16] or ribosomes[55] directly, and eIF4A may therefore possess additional functions outside of its role within eIF4F.

Collectively, our results enable us to propose a model for mRNA activation (Fig. 4). In the first step, eIF4G:E stochastically binds to the mRNA. In the next step, eIF4A attempts to strip eIF4G:E from the mRNA, bifurcating the cycle. If eIF4G:E is bound in a cap-distal, non-productive location, eIF4A is able to eject eIF4G:E from its current binding location by either facilitating hopping to a new location, which we observe both in the presence and absence of eIF4A (Extended Data Fig. 4), on the mRNA or releasing eIF4G:E from the mRNA entirely. However, if eIF4G:E binds near the cap and eIF4E is able to bind to the cap, an eIF4E-dependent conformational change of eIF4G probably renders eIF4A–ATP unable to strip eIF4G:E, trapping the eIF4G:E:A complex at the 5′ cap. This 5′-cap-stalled eIF4F–ATP constitutes the activated state of the mRNA. In the next steps of the mechanism, we speculate that 43S PICs can contact eIF4G:E:A on the activated mRNA and reactivate the strippase modality of eIF4A, as PICs are known to stimulate ATP hydrolysis by eIF4A[11], and while ATP hydrolysis is not required for stripping from uncapped mRNA positions, a single ATP hydrolysis event is both necessary and sufficient to drive mRNA loading[11,49]. This reactivation could then facilitate either a configurational rearrangement or complete exchange of eIF4F with the 43S PIC, which then loads onto the mRNA. This exchange could possibly lead to the direct association between eIF4G and the 48S PIC, an event that has been inferred from in vivo experiments suggesting that a ribosome-bound eIF4F holds onto the cap during scanning[56] and recent structures that observe eIF4F on the exit channel side of the ribosome[55]. As the intracellular concentration of

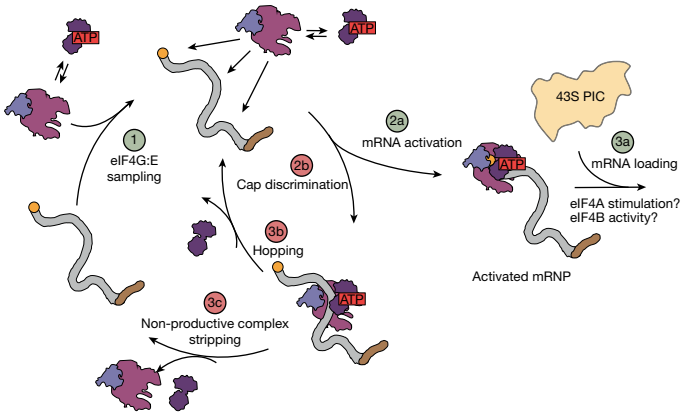

Fig. 4 | The mechanism of mRNA activation. Our experiments lead us to the following model of mRNA activation: in the first step, eIF4G:E non-specifically samples and binds to mRNA. In the second step, the pathway bifurcates into productive (green) or non-productive (red) pathways. In the non-productive fork (2b), eIF4G:E binds far away from the cap, preventing eIF4E from associating with the cap, allowing eIF4A to recycle the eIF4F complex by either facilitating its intramolecular hopping to another place on the same mRNA molecule (3b) or completely removing it from the RNA (3c). In the productive fork (2a), eIF4G:E binds at the 5′ UTR near the cap, and the eIF4E–cap interaction allosterically signals to eIF4A, through eIF4G, not to strip eIF4G. This stalled eIF4F complex at the cap constitutes the previously elusive activated messenger ribonucleoprotein complex (mRNP), in which we speculate eIF4A may be held in an inactive conformation that can be reactivated by an eIF4B-containing 43S PIC before loading the mRNA onto the ribosome (3a). Notably, because eIF4A is present at high concentrations in the cell, this model is agnostic to which step eIF4A binds to eIF4G:E and, owing to its modest affinity, we speculate that it is dynamically sampling the complex throughout the cycle.

eIF4A is very high[6], even its modest affinity to eIF4G enables it to nearly always be bound to eIF4G:E, although it may be constantly exchanging with free eIF4A. Notably, the stochastic sampling of the mRNA by eIF4F that we observed explains early reports that four to five rounds of eIF4F activity are required to facilitate recruitment[3,57] and recent in vivo reports that translation levels occur in oscillating bursts that can be modulated by eIF4F, whereby the ability of eIF4F to diffuse along the mRNA could lead to it being retained on the mRNA for multiple initiation cycles[58]. Notably, eIF4B does not appear to contribute to the mechanistic steps of cap recognition that we observed in this study. However, this finding is consistent with in vivo and biochemical results showing that eIF4B directly interacts with the ribosome, suggesting that it may have a role in downstream steps.

Much effort has gone into looking for mRNA sequences or proteins that regulate eIF4F binding at the 5′ end[3,16,39,50,59] and, although we do not observe a 5′ bias in the system examined here, we cannot exclude the possibility that elements positioned near the cap may have critical regulatory roles, and sequences with which eIF4G poorly binds probably exist[16,59]. However, our results suggest that cells may also regulate the translation efficiency by encoding factors that accelerate the search for the cap, rather than the stability of the resulting activated mRNA, and that consideration of the entire body of the mRNA, and the RNA-binding proteins contained within, is warranted when considering the ability of an mRNA to recruit eIF4F. It is also possible that extreme cap-proximal RNA sequences, which are known to alter the affinity of eIF4E for the cap in the absence of eIF4G[60], also alter the lifetime of the activated state. It is worth emphasizing that the study conducted here used *S. cerevisiae* eIF4F. However, given the nature of the similarities and differences between *S. cerevisiae* and mammalian eIF4F (reviewed previously[3]), we expect the fundamental mechanism that we have described here to generalize to higher eukaryotes, an expectation that must of course be explicitly tested in mammalian systems. Moreover, although our work here focused on cap-dependent translation, cap-independent translation is often eIF4G and eIF4A dependent[7,31]. This suggests that the allosteric communication transduced by cap-bound eIF4E through eIF4G, which has been observed in other contexts[19,32], can be induced by other factors during non-canonical translation initiation.

Online content

Any methods, additional references, Nature Portfolio reporting summaries, source data, extended data, supplementary information, acknowledgements, peer review information; details of author contributions and competing interests; and statements of data and code availability are available at https://doi.org/10.1038/s41586-024-08304-0.

1. Gingras, A. C., Raught, B. & Sonenberg, N. eIF4 initiation factors: effectors of mRNA recruitment to ribosomes and regulators of translation. *Annu. Rev. Biochem.* **68**, 913–963 (1999).
2. Hinnebusch, A. G. & Lorsch, J. R. The mechanism of eukaryotic translation initiation: new insights and challenges. *Cold Spring Harb. Perspect. Biol.* **4**, a011544 (2012).
3. Merrick, W. C. eIF4F: a retrospective. *J. Biol. Chem.* **290**, 24091–24099 (2015).
4. Abramson, R. D. et al. The ATP-dependent interaction of eukaryotic initiation factors with mRNA. *J. Biol. Chem.* **262**, 3826–3832 (1987).
5. Kaye, N. M., Emmett, K. J., Merrick, W. C. & Jankowsky, E. Intrinsic RNA binding by the eukaryotic initiation factor 4F depends on a minimal RNA length but not on the m7G cap. *J. Biol. Chem.* **284**, 17742–17750 (2009).
6. von der Haar, T. & McCarthy, J. E. Intracellular translation initiation factor levels in *Saccharomyces cerevisiae* and their role in cap-complex function. *Mol. Microbiol.* **46**, 531–544 (2002).
7. Martinez-Salas, E., Francisco-Velilla, R., Fernandez-Chamorro, J. & Embarek, A. M. Insights into structural and mechanistic features of viral IRES elements. *Front. Microbiol.* **8**, 2629 (2017).
8. Jia, Y., Polunovsky, V., Bitterman, P. B. & Wagner, C. R. Cap-dependent translation initiation factor eIF4E: an emerging anticancer drug target. *Med. Res. Rev.* **32**, 786–814 (2012).
9. Otero, L. J., Ashe, M. P. & Sachs, A. B. The yeast poly(A)-binding protein Pab1p stimulates in vitro poly(A)-dependent and cap-dependent translation by distinct mechanisms. *EMBO J.* **18**, 3153–3163 (1999).
10. He, H. et al. The yeast eukaryotic initiation factor 4G (eIF4G) HEAT domain interacts with eIF1 and eIF5 and is involved in stringent AUG selection. *Mol. Cell. Biol.* **23**, 5431–5445 (2003).
11. Yourik, P. et al. Yeast eIF4A enhances recruitment of mRNAs regardless of their structural complexity. *eLife* **6**, e31476 (2017).
12. Kumar, P., Hellen, C. U. & Pestova, T. V. Toward the mechanism of eIF4F-mediated ribosomal attachment to mammalian capped mRNAs. *Genes Dev.* **30**, 1573–1588 (2016).
13. Gruner, S. et al. The structures of eIF4E-eIF4G complexes reveal an extended interface to regulate translation initiation. *Mol. Cell* **64**, 467–479 (2016).
14. Oberer, M., Marintchev, A. & Wagner, G. Structural basis for the enhancement of eIF4A helicase activity by eIF4G. *Genes Dev.* **19**, 2212–2223 (2005).
15. Rajagopal, V., Park, E. H., Hinnebusch, A. G. & Lorsch, J. R. Specific domains in yeast translation initiation factor eIF4G strongly bias RNA unwinding activity of the eIF4F complex toward duplexes with 5′-overhangs. *J. Biol. Chem.* **287**, 20301–20312 (2012).
16. Cetin, B. & O'Leary, S. E. mRNA- and factor-driven dynamic variability controls eIF4F-cap recognition for translation initiation. *Nucleic Acids Res.* **50**, 8240–8261 (2022).
17. O'Sullivan, M. H. & Fraser, C. S. Monitoring RNA restructuring in a human cell-free extract reveals eIF4A-dependent and eIF4A-independent unwinding activity. *J. Biol. Chem.* **299**, 104936 (2023).
18. Lanker, S. et al. Interactions of the eIF-4F subunits in the yeast *Saccharomyces cerevisiae*. *J. Biol. Chem.* **267**, 21167–21171 (1992).
19. Feoktistova, K., Tuvshintogs, E., Do, A. & Fraser, C. S. Human eIF4E promotes mRNA restructuring by stimulating eIF4A helicase activity. *Proc. Natl Acad. Sci. USA* **110**, 13339–13344 (2013).
20. Cetin, B., Song, G. J. & O'Leary, S. E. Heterogeneous dynamics of protein-RNA interactions across transcriptome-derived messenger RNA populations. *J. Am. Chem. Soc.* **142**, 21249–21253 (2020).
21. Sokabe, M. & Fraser, C. S. A helicase-independent activity of eIF4A in promoting mRNA recruitment to the human ribosome. *Proc. Natl Acad. Sci. USA* **114**, 6304–6309 (2017).
22. Sen, N. D., Zhou, F., Ingolia, N. T. & Hinnebusch, A. G. Genome-wide analysis of translational efficiency reveals distinct but overlapping functions of yeast DEAD-box RNA helicases Ded1 and eIF4A. *Genome Res.* **25**, 1196–1205 (2015).
23. Harms, U., Andreou, A. Z., Gubaev, A. & Klostermeier, D. eIF4B, eIF4G and RNA regulate eIF4A activity in translation initiation by modulating the eIF4A conformational cycle. *Nucleic Acids Res.* **42**, 7911–7922 (2014).
24. Andreou, A. Z. & Klostermeier, D. eIF4B and eIF4G jointly stimulate eIF4A ATPase and unwinding activities by modulation of the eIF4A conformational cycle. *J. Mol. Biol.* **426**, 51–61 (2014).
25. O'Leary, S. E., Petrov, A., Chen, J. & Puglisi, J. D. Dynamic recognition of the mRNA cap by *Saccharomyces cerevisiae* eIF4E. *Structure* **21**, 2197–2207 (2013).
26. Krause, L., Willing, F., Andreou, A. Z. & Klostermeier, D. The domains of yeast eIF4G, eIF4E and the cap fine-tune eIF4A activities through an intricate network of stimulatory and inhibitory effects. *Nucleic Acids Res.* **50**, 6497–6510 (2022).
27. Schutz, P. et al. Crystal structure of the yeast eIF4A-eIF4G complex: an RNA-helicase controlled by protein-protein interactions. *Proc. Natl Acad. Sci. USA* **105**, 9564–9569 (2008).

28. Rozen, F. et al. Bidirectional RNA helicase activity of eucaryotic translation initiation factors 4A and 4F. *Mol. Cell. Biol.* **10**, 1134–1144 (1990).
29. Ray, B. K. et al. ATP-dependent unwinding of messenger RNA structure by eukaryotic initiation factors. *J. Biol. Chem.* **260**, 7651–7658 (1985).
30. Mitchell, S. F. et al. The 5′-7-methylguanosine cap on eukaryotic mRNAs serves both to stimulate canonical translation initiation and to block an alternative pathway. *Mol. Cell* **39**, 950–962 (2010).
31. Marcotrigiano, J. et al. A conserved HEAT domain within eIF4G directs assembly of the translation initiation machinery. *Mol. Cell* **7**, 193–203 (2001).
32. Hershey, P. E. et al. The Cap-binding protein eIF4E promotes folding of a functional domain of yeast translation initiation factor eIF4G1. *J. Biol. Chem.* **274**, 21297–21304 (1999).
33. Rogers, G. W. Jr, Komar, A. A. & Merrick, W. C. eIF4A: the godfather of the DEAD box helicases. *Prog. Nucleic Acid Res. Mol. Biol.* **72**, 307–331 (2002).
34. Lindqvist, L., Imataka, H. & Pelletier, J. Cap-dependent eukaryotic initiation factor-mRNA interactions probed by cross-linking. *RNA* **14**, 960–969 (2008).
35. Liu, X., Schuessler, P. J., Sahoo, A. & Walker, S. E. Reconstitution and analyses of RNA interactions with eukaryotic translation initiation factors and ribosomal preinitiation complexes. *Methods* **162-163**, 42–53 (2019).
36. Hilbert, M., Kebbel, F., Gubaev, A. & Klostermeier, D. eIF4G stimulates the activity of the DEAD box protein eIF4A by a conformational guidance mechanism. *Nucleic Acids Res.* **39**, 2260–2270 (2011).
37. Andreou, A. Z., Harms, U. & Klostermeier, D. eIF4B stimulates eIF4A ATPase and unwinding activities by direct interaction through its 7-repeats region. *RNA Biol.* **14**, 113–123 (2017).
38. Querido, J. B. et al. The structure of a human translation initiation complex reveals two independent roles for the helicase eIF4A. *Nat. Struct. Mol. Biol.* **31**, 455–464 (2024).
39. Haizel, S. A., Bhardwaj, U., Gonzalez, R. L. Jr, Mitra, S. & Goss, D. J. 5′-UTR recruitment of the translation initiation factor eIF4GI or DAP5 drives cap-independent translation of a subset of human mRNAs. *J. Biol. Chem.* **295**, 11693–11706 (2020).
40. Acker, M. G., Kolitz, S. E., Mitchell, S. F., Nanda, J. S. & Lorsch, J. R. Reconstitution of yeast translation initiation. *Methods Enzymol.* **430**, 111–145 (2007).
41. Wang, J. et al. eIF5B gates the transition from translation initiation to elongation. *Nature* **573**, 605–608 (2019).
42. Jarmoskaite, I., AlSadhan, I., Vaidyanathan, P. P. & Herschlag, D. How to measure and evaluate binding affinities. *eLife* **9**, e57264 (2020).
43. Buttner, L., Javadi-Zarnaghi, F. & Hobartner, C. Site-specific labeling of RNA at internal ribose hydroxyl groups: terbium-assisted deoxyribozymes at work. *J. Am. Chem. Soc.* **136**, 8131–8137 (2014).
44. Graham, J. S., Johnson, R. C. & Marko, J. F. Concentration-dependent exchange accelerates turnover of proteins bound to double-stranded DNA. *Nucleic Acids Res.* **39**, 2249–2259 (2011).
45. Kamar, R. I. et al. Facilitated dissociation of transcription factors from single DNA binding sites. *Proc. Natl Acad. Sci. USA* **114**, E3251–E3257 (2017).
46. Kosar, Z., Attar, A. G. & Erbas, A. Facilitated dissociation of nucleoid-associated proteins from DNA in the bacterial confinement. *Biophys. J.* **121**, 1119–1133 (2022).
47. Luo, Y., North, J. A., Rose, S. D. & Poirier, M. G. Nucleosomes accelerate transcription factor dissociation. *Nucleic Acids Res.* **42**, 3017–3027 (2014).
48. MacDougall, D. D. & Gonzalez, R. L. Jr Translation initiation factor 3 regulates switching between different modes of ribosomal subunit joining. *J. Mol. Biol.* **427**, 1801–1818 (2015).
49. Wang, J. et al. Rapid 40S scanning and its regulation by mRNA structure during eukaryotic translation initiation. *Cell* **185**, 4474–4487 (2022).
50. Rajyaguru, P., She, M. & Parker, R. Scd6 targets eIF4G to repress translation: RGG motif proteins as a class of eIF4G-binding proteins. *Mol. Cell* **45**, 244–254 (2012).
51. Gupta, N., Lorsch, J. R. & Hinnebusch, A. G. Yeast Ded1 promotes 48S translation pre-initiation complex assembly in an mRNA-specific and eIF4F-dependent manner. *eLife* **7**, e38892 (2018).
52. Linder, P. & Jankowsky, E. From unwinding to clamping—the DEAD box RNA helicase family. *Nat. Rev. Mol. Cell Biol.* **12**, 505–516 (2011).
53. Sen, N. D. et al. Functional interplay between DEAD-box RNA helicases Ded1 and Dbp1 in preinitiation complex attachment and scanning on structured mRNAs in vivo. *Nucleic Acids Res.* **47**, 8785–8806 (2019).
54. Sharma, D. & Jankowsky, E. The Ded1/DDX3 subfamily of DEAD-box RNA helicases. *Crit. Rev. Biochem. Mol. Biol.* **49**, 343–360 (2014).
55. Brito Querido, J. et al. The structure of a human translation initiation complex reveals two independent roles for the helicase eIF4A. *Nat. Struct. Mol. Biol.* **31**, 455–464 (2024).
56. Bohlen, J., Fenzl, K., Kramer, G., Bukau, B. & Teleman, A. A. Selective 40S footprinting reveals cap-tethered ribosome scanning in human cells. *Mol. Cell* **79**, 561–574 (2020).
57. Pause, A., Methot, N., Svitkin, Y., Merrick, W. C. & Sonenberg, N. Dominant negative mutants of mammalian translation initiation factor eIF-4A define a critical role for eIF-4F in cap-dependent and cap-independent initiation of translation. *EMBO J.* **13**, 1205–1215 (1994).
58. Livingston, N. M. et al. Bursting translation on single mRNAs in live cells. *Mol. Cell* **83**, 2276–2289 (2023).
59. Zinshteyn, B., Rojas-Duran, M. F. & Gilbert, W. V. Translation initiation factor eIF4G1 preferentially binds yeast transcript leaders containing conserved oligo-uridine motifs. *RNA* **23**, 1365–1375 (2017).
60. Tamarkin-Ben-Harush, A., Vasseur, J. J., Debart, F., Ulitsky, I. & Dikstein, R. Cap-proximal nucleotides via differential eIF4E binding and alternative promoter usage mediate translational response to energy stress. *eLife* **6**, e21907 (2017).

Methods

Expression and purification of non-eIF4G protein factors

Yeast ribosomes and the yeast initiation factors eIF1, eIF1A, eIF4A, eIF4B and eIF4E were expressed and purified from *Escherichia coli* BL21(DE3) RIPL (Agilent) according to established procedures[30,35,40,41]. eIF1, eIF1A, eIF4A and eIF4E were expressed with N-terminal hexahistidine (6×His) tags followed by a Tobacco Etch Virus (TEV) protease cleavage site. eIF4B was expressed with a C-terminal TEV site followed by a 6×His tag. Native, 6×His tagged eIF2 was expressed and purified from *S. cerevisiae* strain GP3511 as previously described[40]. Native, 6×-his-tagged eIF3 was purified from *S. cerevisiae* strain LPY87 according to standard procedures with minor deviations[35]. After affinity purification, rather than phosphocellulose chromatography, eIF3 was applied to a 5 ml HiTrap Q HP column (Cytiva) and its final gel-filtration and storage buffer consisted of 20 mM HEPES, pH 7.4, 200 mM KCl, 10% glycerol and 2 mM dithiothreitol (DTT).

Expression of eIF4G

eIF4G was expressed from a pET28a vector containing a C-terminal TEV protease cleavage site followed by an FH8 tag and 6×His tag. This results in an ENLYQ scar on the C-terminus of eIF4G at the end of purification. In order to express eIF4G, BL21(DE3) RIPL cells were freshly transformed with pET28a-eIF4G and plated on Luria broth (LB) agar plates containing 100 μg ml^{-1} carbenicillin (carb). After transformation, the plates were incubated at 37 °C overnight and then kept at room temperature for up to 10 h until inoculation of overnight cultures in 2.5 l ultrayield flasks (Thomson Instrument Company) containing 500 ml of LB supplemented with carb, 34 μg ml^{-1} chloramphenicol, and 0.6% glucose. Overnight cultures were grown for 14–16 h at 32 °C and then diluted 62.5:1 into 12 l of fresh LB carb + 1% glucose split across 8 ultrayield flasks. The diluted cell culture was grown in a refrigerated shaker with a shaking speed of 215 rpm at 30 °C until it reached an optical density at 600 nm (OD_{600}) of ~0.3 (approximately 2.5 h). The shaker was then shifted to 25 °C while shaking for 1 h. Next, eIF4G expression was induced by addition of 670 μl of freshly prepared 1 M isopropyl β-D-1-thiogalactopyranoside (IPTG) to each flask resulting in a final IPTG concentration of around 0.45 mM. After induction, the temperature of the shaker was set to 22 °C and the cells were allowed to induce for 1 h and 15 min. After induction, cell flasks were immediately moved to a plastic autoclave bin filled with ice and pelleted by repeated centrifugation at 5,500 rcf for 5 min. The pelleted cells were resuspended in ~35 ml of eIF4G lysis buffer (50 mM HEPES pH 7.4, 500 mM KCl, 10% glycerol) crudely measured in a 50 ml conical tube and frozen as droplets by slowly dispensing the resuspended cell culture into liquid nitrogen. The resulting cell 'popcorn' can be stored at −80 °C for at least 2 months. The cell popcorn was then lysed in a freezer mill (SPEX) using 7 cycles of 2 min on-time at a rate of 10 cycles per second, followed by 1 min of off-time. The resulting cell powder was then stored at −80 °C and usable for at least 2 months.

Purification of eIF4G

Cell lysate powder from 12 l of cell culture was resuspended in 300 ml of room temperature eIF4G lysis buffer supplemented with 2 EDTA-free protease inhibitor tablets (Roche), 20 mM imidazole, 10 mM magnesium chloride ($MgCl_2$) and 50 μg of nuclease A from *Serratia marcescens* by slowly adding the powder to actively stirring lysis buffer in a 1 l glass beaker. It takes approximately 20 min to resuspend the cell powder. The lysate was then clarified at 31,500 rcf for 35 min and the supernatant was filtered through a 0.45 μm bottle-top filter before loading onto a chelating column (Cytiva) charged with nickel and pre-equilibrated with eIF4G lysis buffer. eIF4G was eluted from the chelating column using a 10 column volume (c.v.) gradient of eIF4G elution buffer (3:1 eIF4G lysis buffer:2 M imidazole pH 8). The entire peak from the nickel column was pooled and diluted eightfold in 20 mM HEPES-KOH pH 7 and loaded onto the HiRes Capto Q 5/50 column (Cytiva) pre-equilibrated in low ion-exchange buffer (20 mM HEPES-KOH pH 7, 100 mM KOAc, 5% glycerol) and eluted using a 20 c.v. gradient into high ion-exchange buffer (20 mM HEPES-KOH pH 7, 1 M KOAc, 5% glycerol). The elution profile from the HiRes CaptoQ is very broad but monitoring absorbance at both 260 nm and 280 nm allows the fractions containing protein to be separated from contaminating RNA. The RNA-depleted, protein-containing fractions were then pooled and diluted fivefold in 20 mM HEPES-KOH before loading onto a HiRes CaptoS 5/50 column (Cytiva) pre-equilibrated in low ion-exchange buffer and eluted across a biphasic gradient of 0–40% for 15 c.v. followed by 40–100% for 7 c.v. in high ion-exchange buffer. At this step, we routinely collect ~3–4 ml of protein which elutes as a sharp peak around 31 mS cm^{-1} conductivity.

After purification using the HiRes CaptoS, 1/100 (w/w) TEV protease and 4 mM β-mercaptoethanol (BME) was added to the sample, and the sample was moved to a 4 °C refrigerator. TEV protease was then allowed to cleave overnight without agitation. The next morning, 20 mM imidazole was added to the cleavage reaction, and 400 μl of Ni-NTA slurry (Goldbio) equilibrated in low ion-exchange buffer was added to the sample in a 15 ml conical tube. The Ni-NTA beads and protein solution were then mixed by pipetting up and down three times every 3 min for 30 min at room temperature. After allowing uncleaved protein and TEV protease to bind the Ni-NTA beads, the beads and uncleaved protein are removed from the sample by passing over a gravity column. The flowthrough from the gravity column was then diluted to 35 ml using low ion-exchange buffer and filtered through a 0.22 μm syringe filter and loaded back onto the HiRes CaptoS column using the same conditions as earlier in the purification. A ~1 ml elution from this gradient is then pooled and protein concentration was measured using a Bradford assay with bovine serum albumin as a standard before aliquoting into 10 μl single-use aliquots and snap-freezing in liquid nitrogen.

eIF4G:E and eIF4G:E(W104A) were expressed and purified identically to eIF4G with the exception that cells are transformed with both pET28a-eIF4G and a pColA-backbone containing kanamycin resistance and full-length, untagged eIF4E under the control of a T7 promoter. Kanamycin is therefore supplemented in all of the carb-containing medium described for eIF4G above.

Fluorophore labelling

Cy5–eIF4E was prepared by purifying eIF4E(A124C) and labelling with sulfo-Cy5 maleimide (Lumiprobe) as previously described[20,25]. The labelling efficiency for eIF4E was approximately 50% based on the absorbance of protein at 280 nm compared to the absorbance of the dye at 650 nm. eIF4G:E–Cy5 was generated by mixing equimolar ratios of eIF4G with Cy5–eIF4E before aliquoting and snap-freezing in liquid nitrogen.

Cy5–eIF4G/eIF4G:E was prepared by purifying eIF4G/eIF4G:E(S501C) according to the procedure above and subsequently labelling the purified protein by incubating it with a tenfold molar excess of sulfo-Cy5 maleimide at 4 °C overnight. Next, the labelling mixtures were spun threw 0.22 μm benchtop spin filters (Ultrafree-MC, Millipore) and loaded onto the Superdex 200 increase 10/300 GL column (Cytiva) equilibrated in low ion-exchange buffer. The peak containing labelled eIF4G/eIF4G:E was collected and subsequently loaded onto the Capto HiResS 5/50 and further purified using the same procedure as described above. eIF4G and eIF4G:E are estimated to be labelled at 77.5% and 77% efficiencies based on the relative absorbances at 280 nm and 650 nm.

Preparation of mRNAs

The native mRNA *rpl41a* was generated by PCR linearizing the puc19 vector containing the *rpl41a* mRNA sequence downstream of T7 promoter followed by T7 in vitro transcription. The reverse primer for PCR encoded a poly$(A)_{30}$ tail through a poly$(dT)_{28}$ track and two ultimate 2′*O*-methylated uridine bases. Moreover, as a consequence of using a T7 promoter, two G nucleotides were appended to the 5′ end of the

sequence to facilitate transcription. Thus, the final *rpl41a* sequence consisted of two G residues followed by the native *rpl41a* mRNA sequence and a 30-nucleotide poly(A) tail.

The 24-mer used in Extended Data Fig. 2 was generated by PCR linearizing and transcribing the first 45-nucleotides of our *rpl41a* mRNA construct. This 45-mer was then hybridized to a 21-nucleotide DNA fragment containing a 5′ biotin, therefore leaving the first 24-nuceotides—the 5′ UTR of *rpl41a*—single stranded.

All transcribed mRNAs were gel-purified using either 7% (*rpl41a*) or 12% (45-mer) 19:1 acrylamide, 7 M urea-Tris, boric acid, EDTA (TBE) polyacrylamide gels. The mRNAs were capped using the vaccinia virus capping enzyme kit (New England Biolabs) following the manufacturer's protocols. However, the capping reactions were allowed to proceed for 2 h rather than 30 min. Capping reactions were then purified using Monarch RNA clean-up columns (New England Biolabs).

Sequences of mRNA and oligonucleotides

mRNA and oligonucleotide sequences were as follows: *rpl41a* mRNA: GGAGACCACAUCGAUUCAAUCGAAAUGAGAGCCAAGUGGAGAAAG AAGAGAACUAGAAGACUUAAGAGAAAGAGACGGAAGGUGAGAGCCA GAUCCAAAUAAGCGGAUUAUGAGUAAAUAACUCUAAUUUUGUUUU AAAUUCUUUCAAGAGUAUCGUAAUGUCAUUGAUGAAUUAACAUGU UAGUUUCUAUUCUACCUCAUAAUGGAUCUAAAUUGCAUACUAAUCUC ACGGUGGGGUGUAAACCAUUGCCUACUAUUUAUAUAGUGCUUUAU AUAUGUCUCACAUAGUUUAAUCAAUUGUCCGUUUUUUUGAAAAAA AAAAAAAAAAAAAAAAAAAAAAAA; *rpl41a* 24-mer (bases hybridized to DNA oligo are underlined): GGAGACCACATCGATTCAATCGAAATG AGAGCCAAGTGGAGAAAG; *rpl41a* 47-mer internal A93 fragment (bases hybridized to DNA oligo are underlined): GAGACGGAAGGT GAGAGCCAGATCCAAATAAGCGGATTATGAGTAAATAACTCTAATTTTG TTTTAAATTC; *rpl41a* 51-mer (Integrated DNA Technologies): GGAG ACCACATCGATTCAATCGAAATGAGAGCCAAGTGGAGAAAGAAGAGA-FAM; DNA oligo for tethering *rpl41a* (Integrated DNA Technologies): biotin-ACATGTTAATTCATCAATGAC; DNA oligo for tethering 24-mer (Integrated DNA Technologies): biotin-CTTTCTCCACTTGGCTCTCAT; DNA oligo for tethering internal A93 fragment (Integrated DNA Technologies): biotin-GAATTTAAAACAAAATTAGAGTTAT; targeting oligo for labelling *rpl41a* at position 14: CCGTCGCCATCTCCCGTAGGTGA AGGGCTTGAAGGTTCCATTCCCGATGTGGTCTC; targeting oligo for labelling *rpl41a* at position 93: CCGTCGCCATCTCCCGTAGGTGA AGGGCTTGGAGGTTCCATTCCCTGGCTCTCACC; targeting oligo for labelling *rpl41a* at position 211: CCGTCGCCATCTCCCGTAGGTGA AGGGCCAATTGGTTCCATTCCAGATCCATTATGAGG.

Fluorophore labelling of mRNAs

We used a terbium-assisted deoxyribozyme to generate fluorophore-labelled mRNAs as previously described[43]. In brief, in a 500 µl total reaction volume, 10 µM *rpl41a* mRNA was hybridized with 12 µM targeting oligo and 17 µM ribozyme RNA component (rD) by heating to 65 °C for 5 min and slow cooling to room temperature over an hour in 50 mM HEPES pH 7.4, 150 mM sodium chloride (NaCl) and 2 mM KCl. After hybridization, magnesium acetate ($Mg(OAc)_2$) was added to 25 mM followed by the addition of 100 µM terbium(III) chloride and 200 µM ethylenediamine-guanosine-5′-triphosphate (EDA-GTP). The reaction was allowed to proceed for 1 h in a 37 °C water path followed by 3 h at room temperature, and then quenched by addition of 1/10 volume 3 M sodium acetate pH 5.2 and ethanol precipitation. The ethanol precipitate was then resuspended and purified on a denaturing gel as described in the section above.

After purification of the site-specific EDA-GTP–mRNA conjugate, the mRNA was labelled using sulfo-Cy3-*N*-hydroxysuccinimide (Cy3-NHS). To perform fluorophore labelling, the mRNA was adjusted to 20 µM in 200 mM phosphate pH 8.4 containing 20% dimethylsulfoxide (DMSO) and 1 mM Cy3-NHS. The reaction was allowed to proceed for 45 min at room temperature, and then quenched with the addition of 1/10 volume of 3 M sodium acetate pH 5.2. After quenching, excess dye was removed and the phosphate was desalted into 0.3 M sodium acetate using a 5 ml desalting column (Cytiva) and the eluate was ethanol precipitated. The purified, fluorescently labelled RNA was then capped according to the procedure described above.

Assay buffer

All measurements were performed in a standard reaction buffer (20 mM HEPES pH 7.4, 100 mM KOAc, 3 mM $Mg(OAc)_2$) previously determined to facilitate in vitro translation initiation[30,35,40].

mRNA recruitment gel-shift assays

mRNA recruitment gel-shift assays used to monitor a stalled 48S PIC on the start codon of *rpl41a* were performed using previously described standard protocols[11,30,35]. In brief, in vitro transcribed *rpl41a* mRNA was 'hot capped' using a 1:100 ratio of α-P^{32}-GTP–GTP. Mixtures containing the relevant initiation factor mixes (Extended Data Fig. 1b), initiator tRNA, ATP·Mg^{2+}, and 40S ribosomal subunits were assembled, and reactions were started with the addition of hot-capped mRNA. After half an hour, the reactions were quenched by loading into a running native 4% 37.5:1 acrylamide tris, HEPES, EDTA, magnesium (THEM) gel, which was then imaged on a Typhoon 5 (Cytiva) after exposure to a phosphor screen.

Fluorescence anisotropy

For the titration-regime fluorescence anisotropy assays, experiments were performed using a 3′-fluoroscein-modified RNA fragment (Integrated DNA Technologies) consisting of the first 51 nucleotides of our *rpl41a* construct (51-mer-FAM). Reactions (200 µl) were assembled by diluting a 100 µM of 51-mer-FAM to 500 nM or 50 nM in reaction buffer. A total of 200 µl was transferred to a quartz cuvette and small volumes of eIF4G were titrated into the cuvette to generate RNA–eIF4G stoichiometries of 0, 0.2, 0.4, 0.6, 0.8, 1, 1.5, 2, 2.5, 3, 3.5, 4 and 5, or 0, 0.2, 0.4, 0.5, 0.6, 0.8, 1, 1.2, 1.6, 2, 2.5, 3 and 4 for the 500 nM and 50 nM reactions, respectively. The total titration did not change the total reaction volume by more than 10%. After each titration point, the sample was allowed to equilibrate for 5 min, and the fluorescence anisotropy[61] was then measured using vertically polarized excitation light on the Horiba fluorimeter with excitation at 480 nm and emission at 518 nm.

Anisotropy to measure the affinity of eIF4A to the 51-mer-FAM construct was performed using a twelve-point twofold dilution series between 0 and 22 µM eIF4A in reaction buffer supplemented with 2 mM ATP·Mg. These experiments were allowed to equilibrate for 15 min and then measured on measured on the BioTek Synergy Neo2 plate reader (Agilent) using a 485 nm excitation source and an Agilent Green FP filter cube (Agilent, 8040561).

TIRF microscopy

All smFRET experiments were performed on a lab-built, prism-type total internal fluorescence (TIRF) microscope described previously[62,63]. In brief, the samples were excited with a 532 nm laser (gem 532; Laser Quantum) at a power corresponding to 30 mW just before hitting the prism and imaged using an Andor Ultra 888 electron-multiplying charge-coupled device (EMCCD) camera. Videos were collected using an exposure time of 100 ms and were conducted with either continuous excitation by the laser or by mechanically shuttering the laser for 1 frame every 3 s. The experiments for the titration of eIF4A in Extended Data Fig. 8a were performed at 17 °C using a 15 mW laser power and an exposure time of 200 ms. The microscope, camera and accessories were controlled using micromanager[64].

All of the experiments were performed in quartz microfluidic flow-cells passivated with a monolayer of a mixture of methoxy-terminated PEG and biotin-terminated PEG (5,000 kDa, Laysan) as previously described[62,63]. To improve the previously described passivation, we altered the standard PEG-deposition steps to be a one-step passivation

by directly using PEG-silane in cloud-point conditions. The final passivation solution was the bottom layer of a 5% PEG cloud-point solution generated in 1% acetic acid and 750 mM $MgSO_4$, which was allowed to react with the quartz surface in a humidified chamber overnight. The ratio of methoxy-capped PEG to biotin-PEG was 10,000:1.

For all experiments, reaction chambers were prepared by washing the flowcells with reaction buffer, followed by reaction buffer containing 0.1% Tween-20. Tween-20 was then expelled from the flowcell using reaction buffer and 10 nM Streptavidin was allowed to bind to the biotin-PEG for 1 min before being washed out with reaction buffer. RNA molecules were then specifically tethered to the surface, through Streptavidin, by hybridizing a short DNA oligo containing biotin to the middle of *rpl41a*. The mRNA was allowed to bind to the surface for 30 s and then untethered mRNA molecules were expelled by washing the flowcell with reaction buffer. Finally, imaging buffer (reaction buffer supplemented with 1% glucose, 1 μg glucose oxidase, 0.85 μg catalase, 1 mM cyclooctotatraene, 1 mM nitro-benzoic acid, 2 mM trolox aged to 2% oxidation in a 50 μl volume) containing triplet-state quenchers and an oxygen-scavenging system was injected into the flowcell before our injection experiments. For ejection experiments, this imaging buffer also contained whatever protein complex was ejected from the flowcell (discussed in detail in the next section).

smFRET experiments

The association rates for Cy5–eIF4G/eIF4G:E were determined by injecting Cy5–eIF4G/eIF4G:E into flowcells containing capped, uncapped or cap-distal mRNAs at varying concentrations of Cy5–eIF4G/eIF4G:E. The concentration series consisted of 1 nM, 3 nM and 5 nM. The association rates for Cy5–eIF4G:E with either eIF4A or with eIF4A and eIF4B were determined from a single concentration point where 3 nM Cy5–eIF4G:E was mixed with either 2 μM eIF4A and 2 mM ATP or 2 μM eIF4A, 500 nM eIF4B and 2 mM ATP and subsequently injected into the flowcell.

Similarly, the pre-steady-state dissociation rates for Cy5–eIF4G/eIF4G:E were determined by allowing 3 nM Cy5–eIF4G/eIF4G:E to bind the surface-tethered mRNA for 5 min in imaging buffer and then ejecting all free, unbound Cy5–eIF4G/eIF4G:E from the flowcell by exchanging the solution in the flowcell with fresh imaging buffer, which lacked Cy5–eIF4G:E. For experiments containing eIF4A and/or eIF4B, the experiment was performed by ejecting all of the free, unbound Cy5–eIF4G/eIF4G:E using fresh imaging buffer containing 2 μM eIF4A and 2 mM ATP or 2 μM eIF4A, 500 nM eIF4B and 2 mM ATP.

The experiments for the eIF4A titration found in Extended Data Fig. 8a were performed as described above for the pre-steady-state eIF4A injection experiments with the following modifications: the experiments were performed at 17 °C using a 15 mW laser power and an exposure time of 200 ms and varying concentrations of eIF4A, as indicated in the figure, were supplemented into the imaging buffer used for ejection of free eIF4G:E from the uncapped mRNA.

Cy5–eIF4E experiments were performed analogously to those of Cy5–eIF4G:E, except a titration series of 5 nM, 25 nM and 50 nM were used to determine the association rate of Cy5–eIF4E binding to each mRNA construct. As binding was transient, no pre-steady-state experiments for Cy5–eIF4E were performed, but rather the steady-state dissociation rate was used. eIF4G:E–Cy5 injection and ejection experiments were performed at 5 nM to compensate for the lower labelling efficiency of eIF4E-Cy5.

For all non-shuttering injection and ejection experiments, the exchange of solution in the flowcell was started approximately 1.5 s (15 frames) after imaging began. For all of the shuttering experiments, ejection occurred between 3 and 6 s (frames 2 and 3).

Analysis of smFRET data

All analyses of smFRET data were performed using custom-written, in-lab, but publicly available software. Individual trajectories were extracted from videos using vbscope[65], and trajectories were analysed and fit to hidden Markov models using tMAVEN[66], a Python-based software package that integrates single-molecule analysis methodologies that our laboratory has previously published into one software.

For each trajectory, the E_{FRET} was calculated as the acceptor intensity divided by the sum of the donor and acceptor intensities. The signal to background ratio was then calculated for each trajectory, and trajectories with a signal-to-background ratio of less than 5 were removed before analysis. The high signal-to-background ratio trajectories were then visually inspected to look for the characteristics of a single molecule—single-step photobleaching or single step photoblinking. The photobleaching point was then set by the user in tMAVEN[66]. Not all trajectories taken under shuttering conditions photobleached during the time course of the experiment. In this case, molecules were selected that displayed similar photophysical and intensity profiles to the non-shuttering and shuttering trajectories that did photobleach, and the entire trajectory was used. After identification of single molecules and photobleaching or photoblinking, each E_{FRET} trajectory was idealized using a three-state hidden Markov model using the vbFRET algorithm[67]. The Viterbi paths of each trajectory were then clustered using a *k*-means algorithm and reproducibly returned overall E_{FRET} values near 0.05, 0.35 and 0.7 for the 3 states for Cy5–eIF4G:E. These three E_{FRET} states were then simplified into a two-state bound and unbound model by combining the two higher E_{FRET} states into one bound state and leaving the low E_{FRET} state representative of 'unbound' mRNA molecules. Notably, this is equivalent to running the three-state HMM model and then thresholding at an E_{FRET} of 0.25 to separate the bound and unbound states. These final, idealized trajectories were then used to calculate the rates in each experiment.

Rates were calculated using survival analysis of the dwell time distributions in each experiment. For injection experiments, the pre-steady-state association rate was calculated by counting the dwell time points between injection and the first binding event (transition from the low E_{FRET} state to the combined high E_{FRET} state). These dwell time points were then converted to survival probabilities by calculating what fraction of the dwell time points were longer than time, *t*, for all possible *t*. The resultant survival probabilities were then fit with a monoexponential decay function (equation (1)). The rates determined from these exponential fits were then scaled linearly to account for incomplete labelling of our proteins by multiplying the rate determined from the fit by the inverse of the labelling efficiency. Notably, the labelling efficiency of Cy5–eIF4G and Cy5–eIF4G:E, from which most of the conclusions in this work are drawn, are nearly identical, so this correction factor primarily affects the comparison of Cy5–eIF4G:E and eIF4G:E–Cy5.

Similarly, the steady-state dissociation rates were calculated by counting the dwell time points in the bound and unbound states across every transition in the injection experiment, except for the first and last dwells, which correspond to the pre-steady-state event and photobleaching, respectively. These dwell time points were then converted to survival probabilities and fit to biexponential decay functions (equation (2)), because the process reports on both dissociation and facilitated dissociation (Extended Data Fig. 2a). The steady-state rates are population weighted averages of the two phases of the biexponential fit (equation (3)). Consistent with existing literature[16,20,25], all reported rates for Cy5–eIF4E in the absence of eIF4G are steady-state rates, and the reported association rates are the population-weighted average of a biexponential fit.

Similar to the pre-steady-state association rate, the pre-steady-state dissociation rate was calculated by counting all of the dwell times between the ejection event and the first dissociation event (transition from the combined high E_{FRET} state into the low E_{FRET} state). These dwell times were used to calculate survival probabilities, which were fit with a monoexponential decay function (equation (1)). *A* corresponds to the amplitude, *k* is the rate and *t* is time.

$$P = A^* e^{-kt} \quad (1)$$

$$P = A_1 e^{-k_1 t} + A_2 e^{-k_2 t} \quad (2)$$

$$k_{av} = \frac{A_1 k_1 + A_2 k_2}{A_1 + A_2} \quad (3)$$

False colouring of Supplementary Videos

The Supplementary Videos accompanying this Article were false coloured by manually contrasting the 16-bit grey scale raw images to an upper ceiling of ~3,000 and then downsampling to an 8-bit RGB video in ImageJ[68]. Each channel was then manually false coloured in ImageJ[68] by adjusting the colour balance for the red or green channel and sliding the respective colour channel ceiling to a value of 127. This has the effect of giving each Supplementary Video a similar level of brightness, although the videos are included to draw attention to the appearance and disappearance of spots during the depicted ejection/injection experiments, and the relative brightness of the spots is not relevant to the conclusions of the manuscript.

Statistical analyses

The titration-regime fluorescence anisotropy experiments were performed once for each concentration.

All single-molecule experiments were performed as two biological replicates and nearly every individual single-molecule experiment contained >100 trajectories from which survival probabilities could be determined. However, experiments with low single-to-noise or trajectory numbers were repeated three times; these experiments were as follows: ejection of Cy5–eIF4G:E from the cap-distal mRNA, and ejection of Cy5–eIF4G:E from the cap-distal mRNA using buffer supplemented with eIF4A and ATP. The titration-regime anisotropy experiments were performed once at each concentration of RNA. Ejection of eIF4G:E from the second cap-distal construct was performed four times due to its low labelling efficiency and therefore low trace counts.

The association rates for Cy5–eIF4G/eIF4G:E and Cy5–eIF4E with the mRNA (Figs. 1 and 2) were determined by fitting the concentration-dependent association rates from individual experiments in the concentration series to a line. The reported rates for those experiments are the slopes of the lines and the errors are errors of the fit. All other reported rates are the means of the replicates, and the errors are the s.d. of those replicates. The raw datapoints used to determine the mean and s.d. are plotted on each bar plot.

mRNA recruitment reactions (raw gel images can be found in Supplementary Fig. 1) and the anisotropy affinity measurement of eIF4A to mRNA were repeated three times.

The number of trajectories used, the number of events in the fit and all of the fitting parameters for the survival-analysis of every single-molecule experiment are provided in Supplementary Table 1.

Reporting summary

Further information on research design is available in the Nature Portfolio Reporting Summary linked to this article.

Data availability

All data analysed in this study are available in the Article and its Supplementary Information. The number of molecules included and the parameters for the raw survival curve fit for each replicate, uncorrected for framerate and labelling efficiency are provided in Supplementary Table 1. The large, raw video files are available on request from the corresponding author.

Code availability

The code used in this study is freely available at our group's GitHub page (vbSCOPE, https://github.com/GonzalezBiophysicsLab/vbscope-paper; tMAVEN, https://github.com/GonzalezBiophysicsLab/tmaven).

61. Lakowicz, J. R. *Principles of Fluorescence Spectroscopy* 3rd edn (Springer, 2006).
62. Blanchard, S. C., Kim, H. D., Gonzalez, R. L. Jr, Puglisi, J. D. & Chu, S. tRNA dynamics on the ribosome during translation. *Proc. Natl Acad. Sci. USA* **101**, 12893–12898 (2004).
63. Blanchard, S. C., Gonzalez, R. L., Kim, H. D., Chu, S. & Puglisi, J. D. tRNA selection and kinetic proofreading in translation. *Nat. Struct. Mol. Biol.* **11**, 1008–1014 (2004).
64. Edelstein, A., Amodaj, N., Hoover, K., Vale, R. & Stuurman, N. Computer control of microscopes using microManager. *Curr. Protoc. Mol. Biol.* https://doi.org/10.1002/0471142727.mb1420s92 (2010).
65. Ray, K. K. et al. Entropic control of the free-energy landscape of an archetypal biomolecular machine. *Proc. Natl Acad. Sci. USA* **120**, e2220591120 (2023).
66. Verma, A. R. et al. Increasing the accuracy of single-molecule data analysis using tMAVEN. *Biophys J.* **123**, 2765–2780 (2024).
67. Bronson, J. E., Fei, J., Hofman, J. M., Gonzalez, R. L. Jr & Wiggins, C. H. Learning rates and states from biophysical time series: a Bayesian approach to model selection and single-molecule FRET data. *Biophys. J.* **97**, 3196–3205 (2009).
68. Schindelin, J. et al. Fiji: an open-source platform for biological-image analysis. *Nat. Methods* **9**, 676–682 (2012).

Acknowledgements This work was supported by funds to R.L.G. from the NIH (5R01GM084288 and CA277727). R.C.G. and N.A.I. were supported by NSF GRFP fellowships (DGE, 1644869). E.W.H. was funded through an F32 fellowship from the NIH (GM139360). Access to the Horiba Fluorimeter was enabled through NSF award 1828491. We thank the staff at the Columbia Precision Biomolecular Characterization Facility for access to equipment.

Author contributions This work was conceptualized by R.L.G. and R.C.G. The single-molecule experiments were performed, analysed and interpreted by R.C.G. with input from R.L.G. and N.A.I. The mRNA recruitment gel-shift experiments were performed, analysed and interpreted by N.A.I. with input from R.L.G. and R.C.G. R.C.G. and N.A.I. generated the materials with contributions from V.M.C. and E.W.H. The improved surface passivation was conceptualized by C.D.K.-T. and performed by R.C.G. R.L.G and R.C.G. wrote the paper.

Competing interests The authors declare no competing interests.

Additional information

Supplementary information The online version contains supplementary material available at https://doi.org/10.1038/s41586-024-08304-0.

Correspondence and requests for materials should be addressed to Ruben L. Gonzalez.

Peer review information *Nature* thanks the anonymous reviewers for their contribution to the peer review of this work. Peer reviewer reports are available.

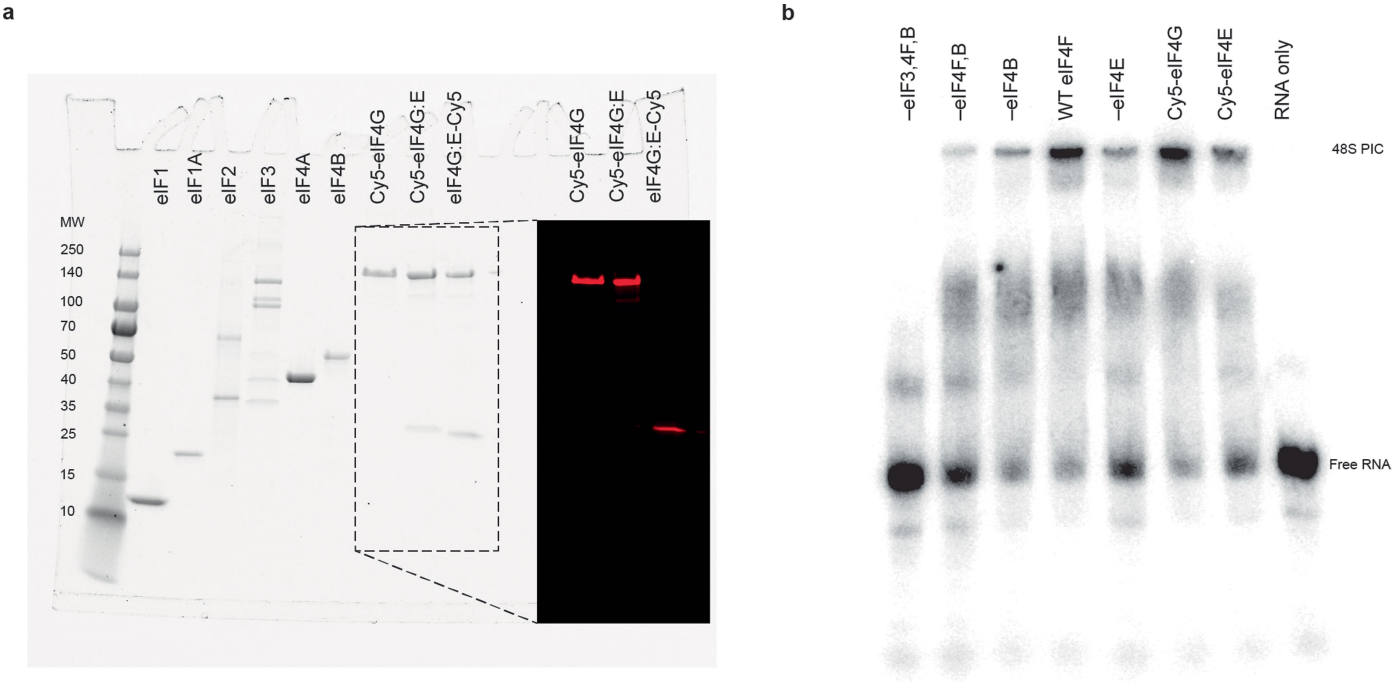

Extended Data Fig. 1 | Purification, labelling, and validation of biochemical components. (a) SDS-PAGE gel showing all of the purified eIFs required to perform mRNA recruitment gel-shift assays. The inset shows a red fluorescence scan of the outlined portion of the SDS-PAGE gel demonstrating that the factors are fluorescently labelled. n = 1 experiment. **(b)** Standard mRNA recruitment gel-shift assay showing recruitment of mRNA onto a stable 48S-PIC in the presence of eIF4F. As expected, diminished recruitment is observed in the absence of eIF4B or eIF4E. n = 1 experiment. **(c)** Titration-regime, anisotropy-based RNA binding experiments performed with either 500 nM or 50 nM FAM-labelled, 51-nucleotide rpl41a fragment. These experiments show that anisotropy continues to increase beyond a 1:1 molar ratio of mRNA:eIF4G, confirming multiple eIF4G molecules bind the short RNA, as previously observed. Each titration-regime experiment was performed once. Gel source data can be found in Supplementary Fig. 1.

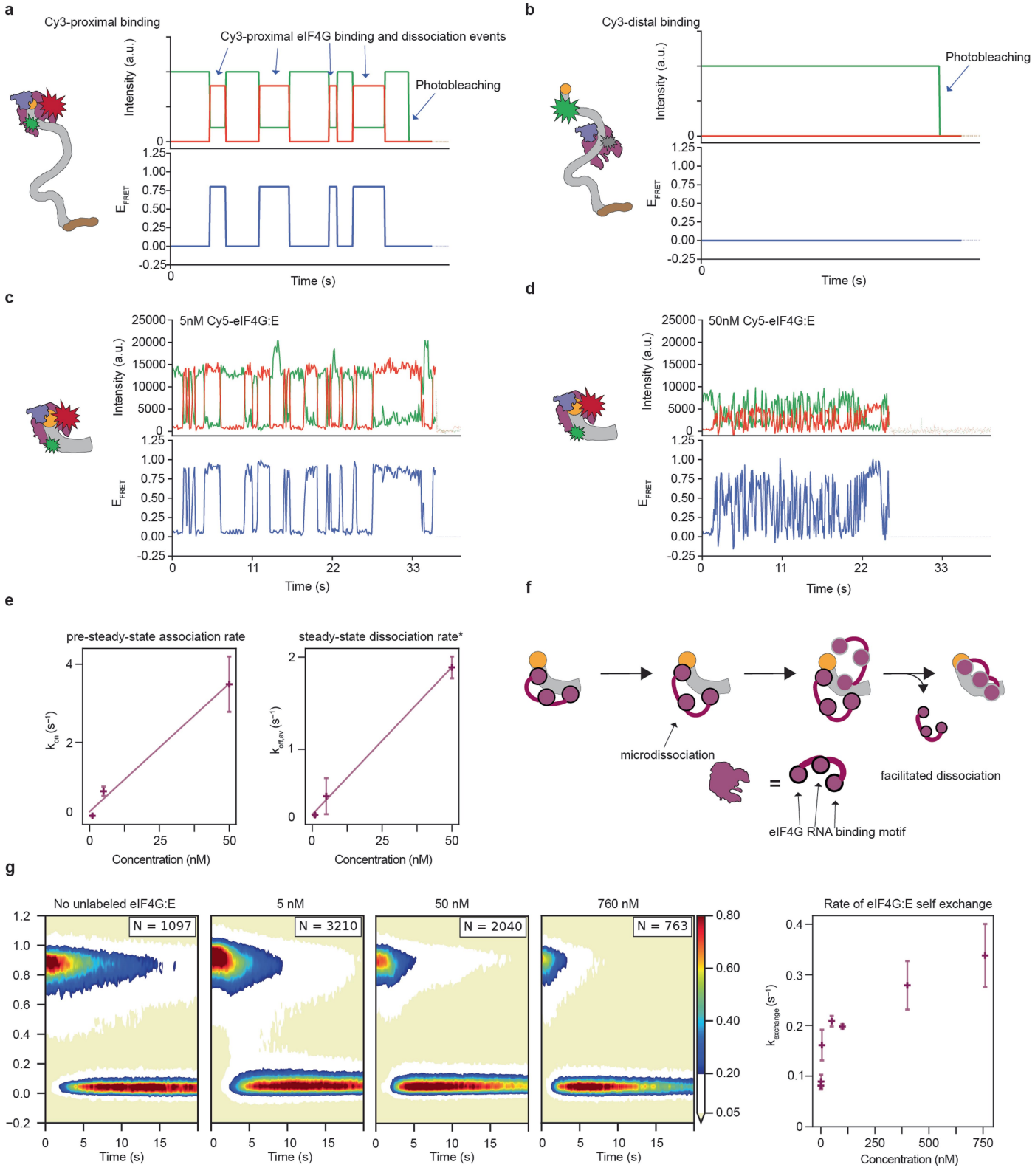

Extended Data Fig. 2 | See next page for caption.

Extended Data Fig. 2 | Validation of smFRET between Cy5-eIF4G:E and Cy3-mRNA. (a) Hypothetical intensities/FRET trajectories showing what is expected to happen if Cy5-eIF4G:E binds at a cap-proximal location on the capped mRNA construct. Upon binding, the green fluorescence intensity decreases while the red intensity increases for the duration of the binding event, leading to an increase in E_{FRET} while Cy5-eIF4G:E is bound near the donor fluorophore. **(b)** Shows similar hypothetical trajectories, but in these trajectories Cy5-eIF4G:E binds at a cap-distal location far away from the donor fluorophore. Because the acceptor and donor fluorophores are not near each other, no changes in intensity or E_{FRET} are detected before photobleaching. **(c)** Shows an example experimental trajectory for Cy5-eIF4G:E binding to the short, capped 24-nucleotide 5′ UTR of rpl41a. Because the RNA is short, we expect only a single binding site. At 5 nM, we observe transient binding, but at 50 nM **(d)**, both the association and dissociation kinetics increase, indicating that eIF4G is able to facilitate its own dissociation. **(e)** Quantification of the concentration dependent pre-steady-state association rate and population weighted average dissociation rate of eIF4G:E from the capped, 24 nucleotide construct, which indicates facilitated dissociation is occurring. Facilitated dissociation is cartooned in **(f)** whereby the release of one of RNA binding domains of eIF4G, also called microdissociation, opens up a binding location for a new molecule of eIF4G, which then facilitates the release of the first eIF4G molecule. **(g)** 2D histograms showing the concentration dependent exchange of Cy5-eIF4G:E bound to the capped, 24-nucleotide construct when increasing concentrations of unlabelled eIF4G:E are injected into the flowcell and quantification to the right. PBL denotes photobleaching limited dissociation rates. n = 2 biological experiments for the experiments in **(e)** and **(g)**; data are presented as means and error bars correspond to standard deviations.

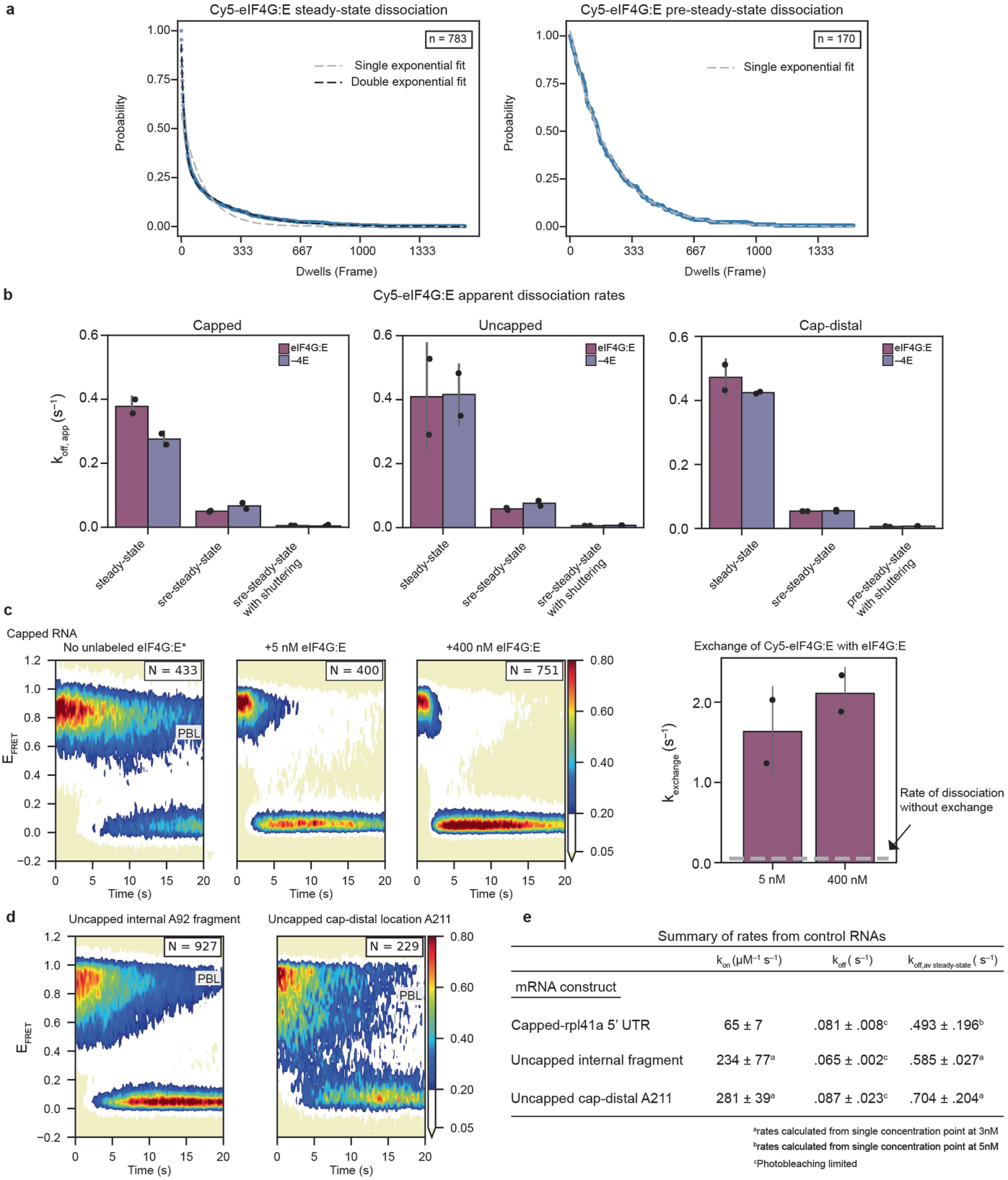

e

Summary of rates from control RNAs

mRNA construct	k_{on} (μM^{-1} s^{-1})	k_{off} (s^{-1})	$k_{off,av\ steady\text{-}state}$ (s^{-1})
Capped-rpl41a 5' UTR	65 ± 7	.081 ± .008[c]	.493 ± .196[b]
Uncapped internal fragment	234 ± 77[a]	.065 ± .002[c]	.585 ± .027[a]
Uncapped cap-distal A211	281 ± 39[a]	.087 ± .023[c]	.704 ± .204[a]

[a]rates calculated from single concentration point at 3nM
[b]rates calculated from single concentration point at 5nM
[c]Photobleaching limited

Extended Data Fig. 3 | See next page for caption.

Extended Data Fig. 3 | Cy5-eIF4G:E facilitates its own dissociation on full-length rpl41a mRNA. (a) Survival-time analysis showing that the steady-state dissociation (left) of Cy5-eIF4G:E on the capped mRNA construct is biphasic, whereas the pre-steady-state dissociation rate (right) is monophasic, indicating that steady-state dissociation events are a mixture of facilitated and non-facilitated dissociation events. **(b)** Comparison of the rate constants derived from steady-state and pre-steady-state experiments indicate facilitated dissociation by eIF4G. Thus, pre-steady-state experiments are more reflective of the inherent dissociation rate of eIF4G:E. Comparison of the pre-steady-state dissociation rates recorded with and without shuttering of the excitation light reveals that dissociation of eIF4G:E is limited by photobleaching. The steady-state dissociation rates plotted are population weighted averages of the two phases shown in **(a)**. n = 2 biological experiments experiment for each condition. **(c)** The ability of unlabelled eIF4G:E to exchange with pre-associated Cy5-labelled eIF4G:E on the capped full-length rpl41a mRNA construct is tested by injecting 5 nM or 400 nM unlabelled eIF4G:E into the flowcell after allowing Cy5-eIF4G:E to bind. *The 2D histogram showing the ejection of free eIF4G:E from the flowcell is repeated from Fig. 1 and Fig. 3 in the main text for comparison. n = 2 biological experiments for each condition. **(d)** 2D histograms showing the photobleaching limited dissociation of Cy5-eIF4G:E from an uncapped fragment of rpl41a encompassing the first cap-distal position on the mRNA (left) and the photobleaching limited dissociation from a second internal labelling position on full-length mRNA after ejection of all free Cy5-eIF4G:E with buffer. **(e)** A summary of the association and dissociation kinetics for the 24-nucleotide 5′ UTR fragment, internal fragment around the cap-distal fluorophore, and a second cap-distal location. PBL denotes photobleaching limited dissociation rates. All data in this figure are presented as means and all error bars correspond to standard deviations.

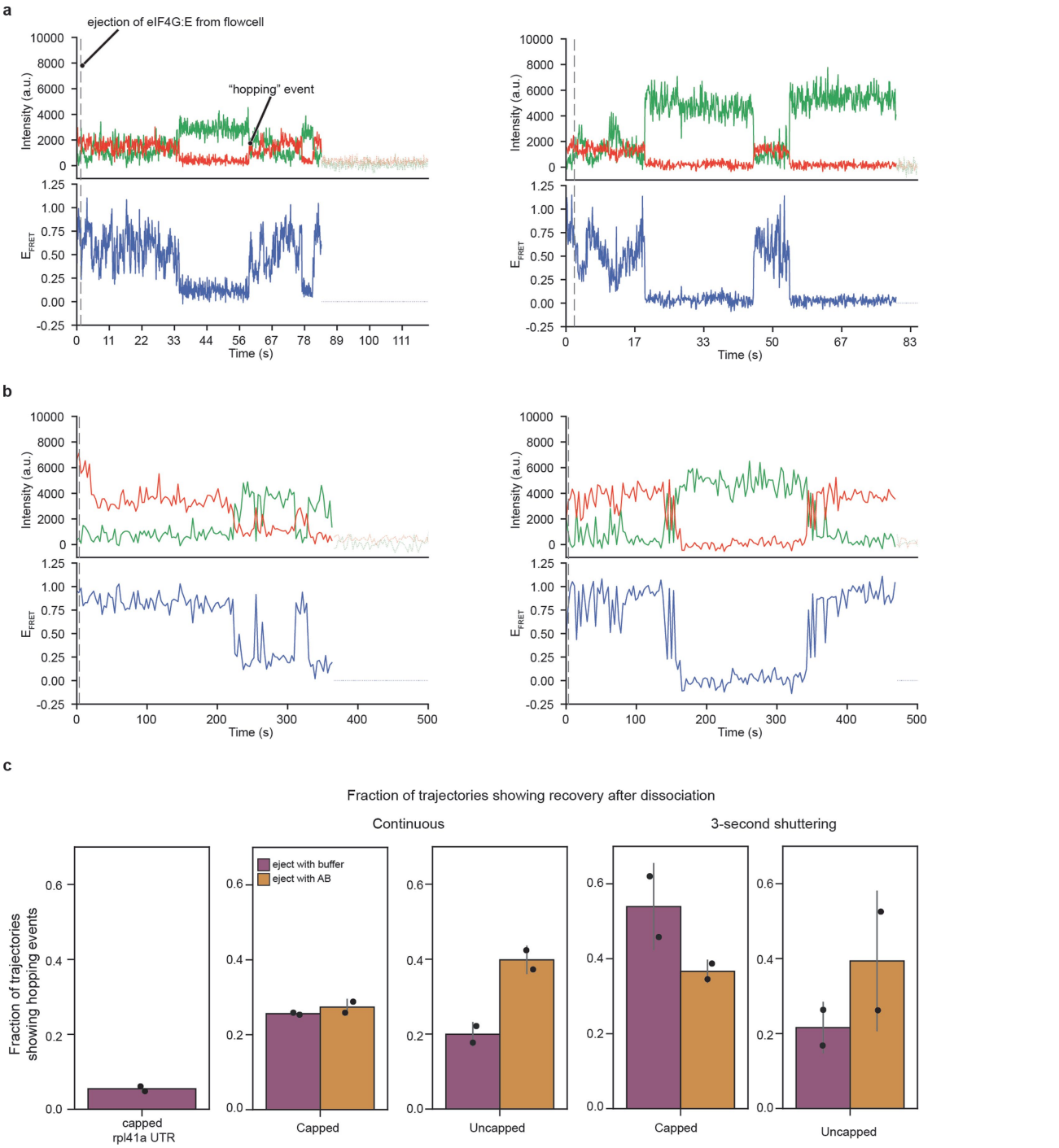

Extended Data Fig. 4 | eIF4G:E can "hop" along an mRNA. Example trajectories taken from pre-steady-state ejection experiments on the capped construct where Cy5-eIF4G:E dissociates from the local position on the mRNA, causing E_{FRET} to drop to 0, but later recovers, despite the all free eIF4G:E being removed from the flowcell, when the same, or another eIF4G:E bound elsewhere on the mRNA, microdissociates and then "hops" to the local position near the donor fluorphore on the mRNA. These example trajectories are shown for both continuous illumination **(a)** and excitation light shuttering **(b)** experiments. **(c)** The fraction of trajectories which contain hopping events is quantified for the capped and uncapped mRNA constructs as a function of ejection with buffer, ejection with buffer supplemented with eIF4A+B + ATP, and shuttering interval. Comparison of the hopping events to a control experiment performed on the capped, 5′ UTR of rpl41a which is too small to contain a second eIF4G binding site with which eIF4G could hop to and from reveals that hopping is prevalent on rpl41a. n = 2 biological experiments for each condition. Data are presented as means and error bars correspond to standard deviations.

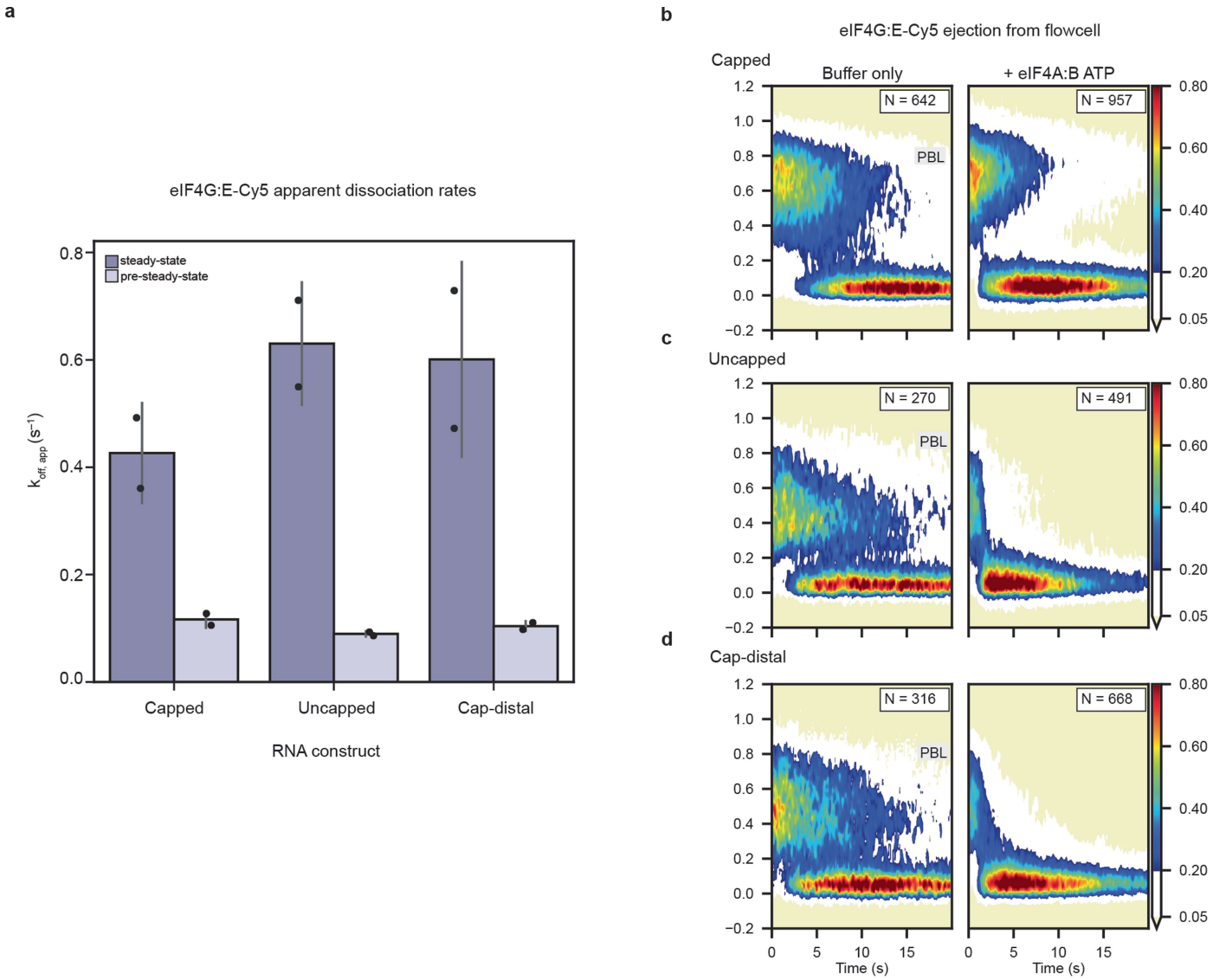

Extended Data Fig. 5 | eIF4G:E-Cy5 facilitates its own dissociation. (a) A bar graph showing the population-weighted average, steady-state dissociation rate of eIF4G:E compared to the pre-steady-state dissociation rate. Similar to Cy5-eIF4G/G:E, free, unbound, eIF4G:E-Cy5 is able to exchange with bound eIF4G:E-Cy5 leading to an increased apparent dissociation rate in steady-state experiments. This serves as additional evidence that eIF4G and eIF4E function as a complex. n = 2 biological experiments for each condition. Data are presented as means and error bars correspond to standard deviations. **(b-d)** The equivalent ejection experiments shown in Fig. 4 but with the acceptor fluorophore on eIF4E instead of eIF4G. Similar to with Cy5-eIF4G:E, eIF4G:E-Cy5 is stripped from every position except from the cap. This demonstrates that eIF4G:E is stripped as a complex during the search for the cap. PBL denotes photobleaching limited dissociation rates.

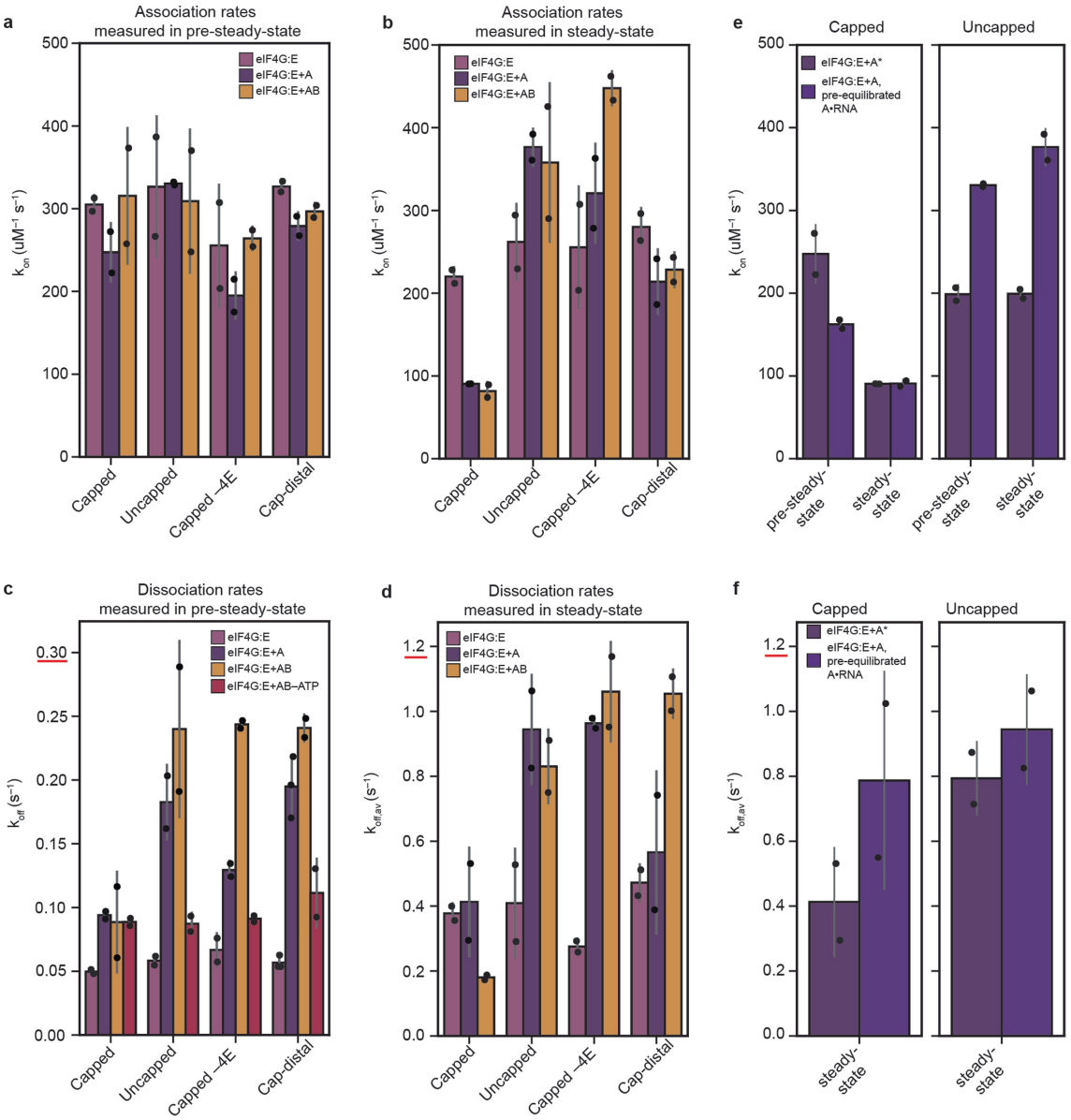

Extended Data Fig. 6 | Association and dissociation kinetics of Cy5-eIF4G:E in the presence of eIF4A and eIF4B. (a) The pre-steady-state association rates calculated from a Cy5-eIF4G:E concentration series, also plotted in Fig. 1, and the pre-steady-state association rates calculated from a single Cy5-eIF4G:E concentration point of 3 nM in the presence of saturating eIF4A+ATP or eIF4A + eIF4B+ATP. eIF4A and eIF4B do not appear to alter the association kinetics. **(b)** The equivalent steady-state association kinetics for the experiments described in **(a)**. **(c)** The steady-state dissociation kinetics calculated from the steady-state portion of the injection experiments for eIF4G:E, eIF4G:E + eIF4A+ATP, and eIF4G:E + eIF4A + eIF4B+ATP. eIF4A and eIF4B enhance the steady-state dissociation rate on every construct except the capped construct in the presence of eIF4E. **(d)** The equivalent pre-steady-state experiment for those described in **(c)**. eIF4A destabilizes eIF4G/G:E from each mRNA construct in an ATP-dependent manner except in the presence of both eIF4E and the cap. A red line at the highest tick mark on the Y-axis of **(b)** and **(c)** denotes the change in axis scale between the two graphs—highlighting that the steady-state dissociation rate far exceeds the pre-steady-state dissociation rate due to facilitated dissociation. **(e-f)** Similar experiments were performed as described in **(a)** and **(c)** except 2 μM eIF4A•ATP was allowed to bind the mRNA prior to the injection of the eIF4F complex. *The data denoted corresponds to the same corresponding data for eIF4G:E + A plotted in **(a-d)** to serve as a direct comparison with and without pre-equilibration of eIF4A on the mRNA. For **(a)**–**(f)** n = 2 biological experiments for each experimental condition; data are presented as means and error bars correspond to standard deviations.

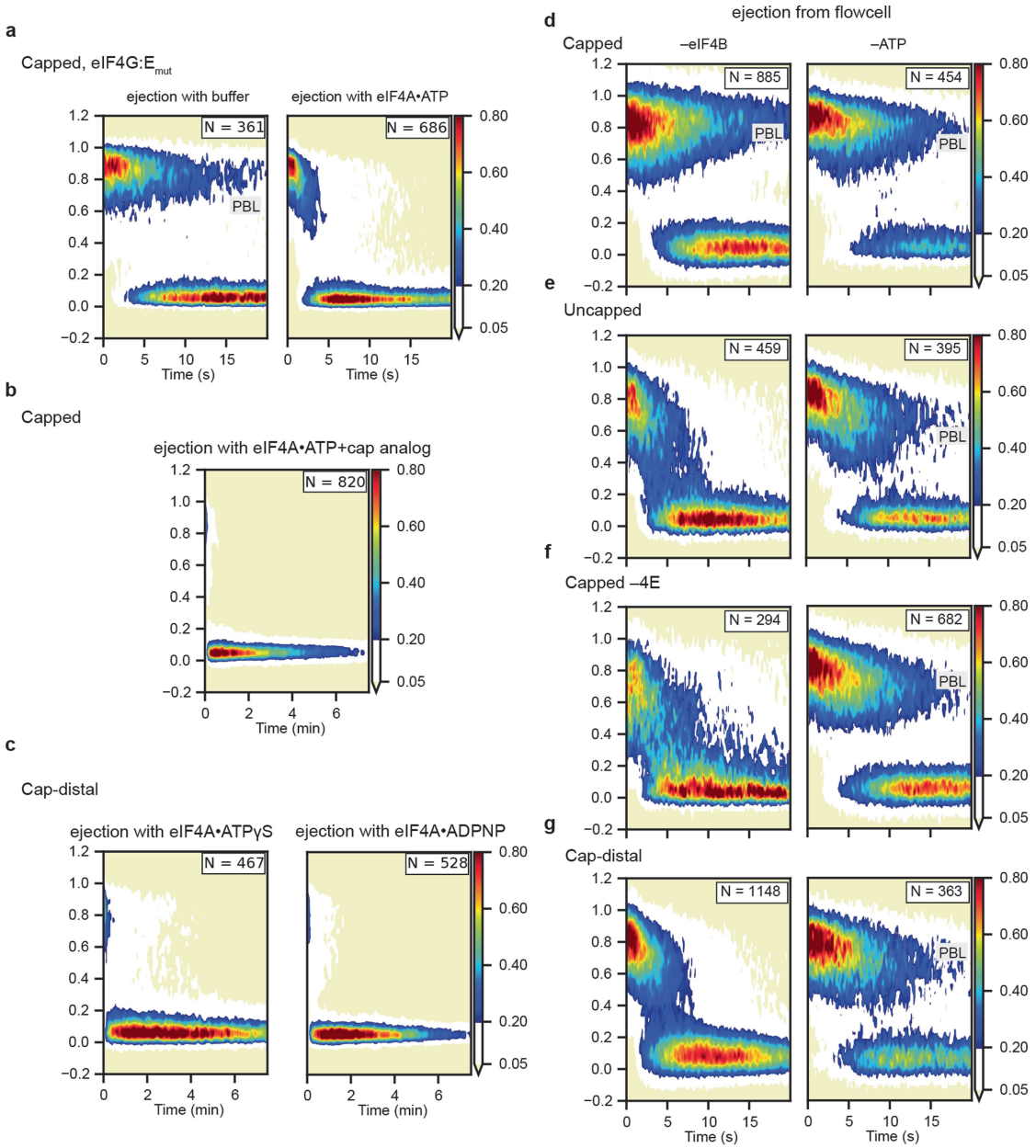

Extended Data Fig. 7 | ATP binding, but not hydrolysis, or eIF4B is required for stripping eIF4G from mRNA. To further validate that the only thing preventing the stripping activity of eIF4A is recognition of the cap by eIF4E, we utilized a mutant of eIF4G:E$_{W104A}$ in which one of the critical tryptophan residues involved in cap recognition is mutated to alanine, thus diminishing the affinity of eIF4E to the cap. eIF4A was effectively able to remove eIF4G from capped positions when cap-recognition was perturbed with these mutations or by competing for cap binding with 200 μM cap analogue m^{7}GpppA **(b)**. eIF4A does not require ATP hydrolysis **(c)** or eIF4B **(d-g)** but does require ATP binding for its strippase activity **(d-g)**. PBL denotes photobleaching limited off rates.

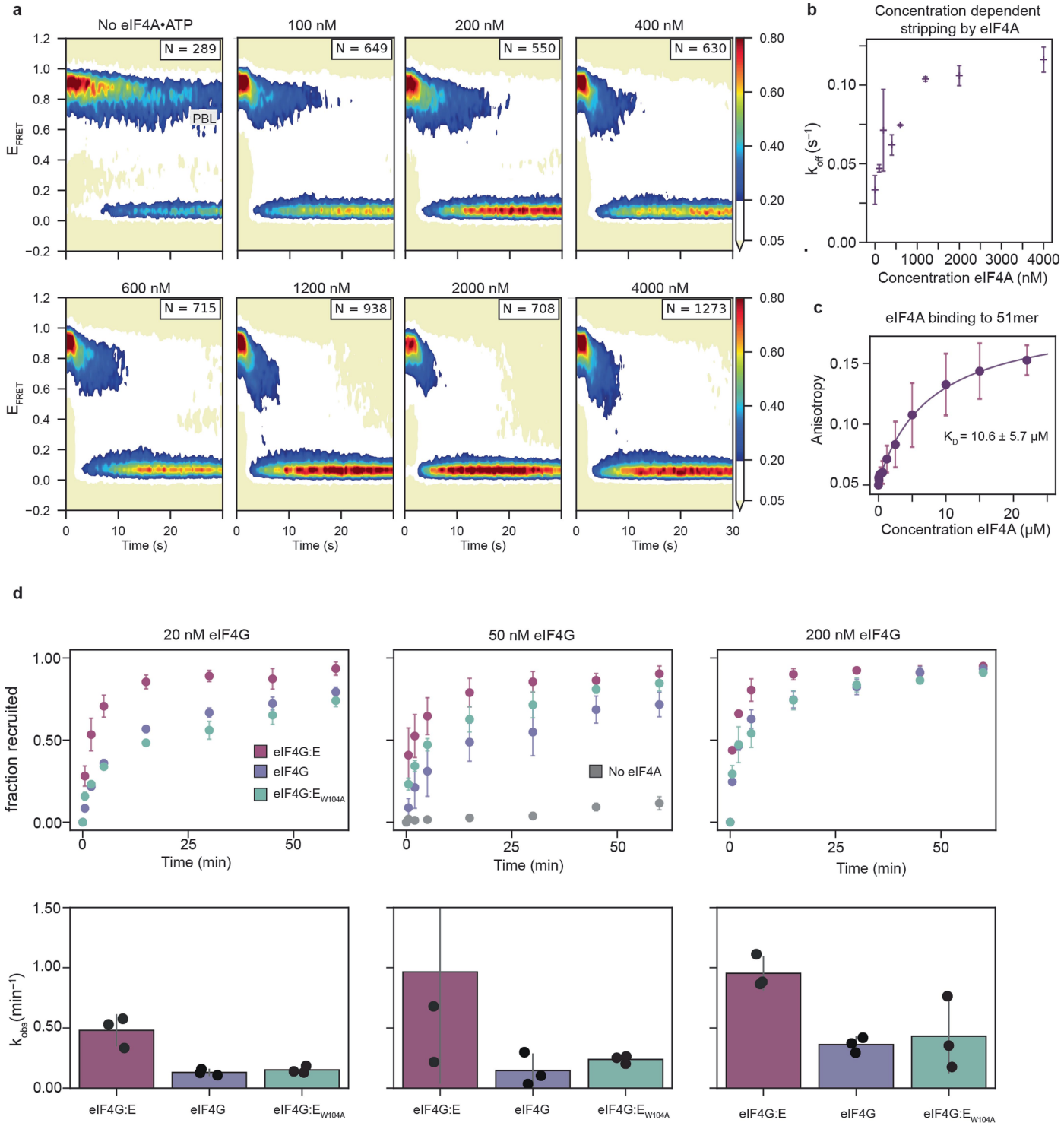

Extended Data Fig. 8 | Direct interaction between eIF4G and eIF4A drives the strippase activity of eIF4A and facilitates mRNA recruitment. (a) 2D histograms illustrating the concentration dependence of stripping eIF4G:E from uncapped mRNA as a function of eIF4A concentration performed at 17 °C and acquired with a 200 ms exposure time, quantified in **(b)**. The half-maximal stripping velocity is achieved between 100–200 nM eIF4A whereas the K_D of eIF4A to the 51mer 5′ fragment of rpl41a in the absence of eIF4G is ~10 µM as measured by fluorescence anisotropy. n = 2 biological experiments for each concentration. **(c)** This illustrates that eIF4A must bind eIF4G to facilitate stripping. n = 3 biological experiments. **(d)** 48S mRNA recruitment reaction time course (top) and quantification (bottom) show that eIF4A is essential for in vitro mRNA recruitment, and that perturbation of cap-recognition by either removal of eIF4E from the reaction or mutation of $eIF4E_{W104A}$ to perturb cap binding results in a rate defect which can be compensated for by increasing concentration of eIF4G. n = 3 biological experiments for each mRNA recruitment condition. Gel source data can be found in Supplementary Fig. 1. All quantified data in this figure are presented as means, and error bars correspond to standard deviations.

Extended Data Table 1 | Comparison of Cy5-eIF4G and Cy5-eIF4E results

Association rate constants measured in pre-steady-state, k_{on} (uM^{-1} S^{-1})

	Cy5-4G:E	4G:E-Cy5
mRNA construct		
Capped –4E	237 ± 41	N.D.
Capped	316 ± 5	271 ± 30[a]
Uncapped	334 ± 5	294 ± 48[a]
Cap-distal	256 ± 39	253 ± 17[a]

Dissociation rate constants measured in pre-steady-state, k_{off} (s^{-1})

	Cy5-4G:E	4G:E-Cy5	Cy5-4G:E:AB	4G:E-Cy5:AB
mRNA construct				
Capped –4E	0.067 ± .013[b]	N.D.	0.244 ± .004	N.D.
Capped	0.050 ± .002[b]	0.116 ± .015[b]	0.088 ± .039[b]	0.165 ± .006[b]
Uncapped	0.057 ± .005[b]	0.090 ± .005[b]	0.240 ± .069	0.590 ± .049
Cap-distal	0.058 ± .005[b]	0.104 ± .009[b]	0.241 ± .011	0.373 ± .008

This table displays a comparison of experiments performed with fluorophore labels on either eIF4G or eIF4E. Association rates are shown on the top and dissociation rates are shown on the bottom. These results reveal that monitoring eIF4G binding to mRNA or eIF4E binding to mRNA report on the same interaction, indicating that eIF4G:E behaves as a bimolecular complex that samples mRNA together, irrespective of the cap. [a]These rates were calculated from a single concentration point at 5 nM. [b]These rates were calculated from experiments collected under continuous laser illumination, and the rates are photobleaching limited.

Extended Data Table 2 | Summary of rate constants

Summary of rate constants

	k_{on} (uM^{-1})	k_{off} (s^{-1})	K_D (pM)
Capped			
eIF4G	237 ± 40[a]	0.0074 ± 0.0003[b]	31 ± 5
eIF4G:E	316 ± 5[a]	0.0050 ± 0.0004[b]	16 ± 1
eIF4G:E+A	247 ± 35[a]	0.0146 ± 0.0046[b]	45 ± 16
eIF4G:E+A+B	315 ± 81[a]	0.0144 ± 0.0009[b]	46 ± 12
eIF4G+A	194 ± 28[a]	0.1293 ± 0.0073[a]	664 ± 103
eIF4G+A+B	264 ± 14[a]	0.2436 ± 0.0043[a]	922 ± 52
Uncapped			
eIF4G	149 ± 7[a]	0.0069 ± 0.0002[b]	46 ± 3
eIF4G:E	334 ± 5[a]	0.0057 ± 0.0001[b]	17 ± 1
eIF4G:E+A	330 ± 3[a]	0.1823 ± 0.0293[a]	553 ± 89
eIF4G:E+A+B	309 ± 87[a]	0.2399 ± 0.0691[a]	776 ± 312
Cap-distal			
eIF4G	277 ± 33[a]	0.0066 ± 0.0012[b]	24 ± 5
eIF4G:E	256 ± 39[a]	0.0057 ± 0.0016[b]	22 ± 7
eIF4G:E+A	279 ± 17[a]	0.1949 ± 0.0241[a]	698 ± 96
eIF4G:E+A+B	297 ± 10[a]	0.2408 ± 0.0105[a]	812 ± 45

This table encompasses a summary of the rate constants measured in this body of work. These rates reveal that eIF4A stimulates the dissociation of eIF4G:E from uncapped positions, but the complex is stabilized at the cap. [a]These rates are calculated from movies with a framerate of 10 frames per second (fps). [b]These rates were calculated from movies with a framerate of 1/3 fps.

nature portfolio

Corresponding author(s): Ruben L. Gonzalez, Jr.

Last updated by author(s): 10/11/2024

Reporting Summary

Nature Portfolio wishes to improve the reproducibility of the work that we publish. This form provides structure for consistency and transparency in reporting. For further information on Nature Portfolio policies, see our Editorial Policies and the Editorial Policy Checklist.

Statistics

For all statistical analyses, confirm that the following items are present in the figure legend, table legend, main text, or Methods section.

n/a	Confirmed	
☐	☒	The exact sample size (*n*) for each experimental group/condition, given as a discrete number and unit of measurement
☐	☒	A statement on whether measurements were taken from distinct samples or whether the same sample was measured repeatedly
☒	☐	The statistical test(s) used AND whether they are one- or two-sided *Only common tests should be described solely by name; describe more complex techniques in the Methods section.*
☒	☐	A description of all covariates tested
☒	☐	A description of any assumptions or corrections, such as tests of normality and adjustment for multiple comparisons
☐	☒	A full description of the statistical parameters including central tendency (e.g. means) or other basic estimates (e.g. regression coefficient) AND variation (e.g. standard deviation) or associated estimates of uncertainty (e.g. confidence intervals)
☒	☐	For null hypothesis testing, the test statistic (e.g. *F*, *t*, *r*) with confidence intervals, effect sizes, degrees of freedom and *P* value noted *Give P values as exact values whenever suitable.*
☒	☐	For Bayesian analysis, information on the choice of priors and Markov chain Monte Carlo settings
☒	☐	For hierarchical and complex designs, identification of the appropriate level for tests and full reporting of outcomes
☒	☐	Estimates of effect sizes (e.g. Cohen's *d*, Pearson's *r*), indicating how they were calculated

Our web collection on statistics for biologists contains articles on many of the points above.

Software and code

Policy information about availability of computer code

Data collection	The freely available software, micromanager version 1.4 (https://micro-manager.org), was used to operate the microscope system and collect the movie files.
Data analysis	All data was analyzed using python 3.10 based, lab-built software freely available on the lab's github page. vbscope: https://github.com/GonzalezBiophysicsLab/vbscope-paper tMAVEN: https://github.com/GonzalezBiophysicsLab/tmaven

For manuscripts utilizing custom algorithms or software that are central to the research but not yet described in published literature, software must be made available to editors and reviewers. We strongly encourage code deposition in a community repository (e.g. GitHub). See the Nature Portfolio guidelines for submitting code & software for further information.

Data

Policy information about availability of data

All manuscripts must include a data availability statement. This statement should provide the following information, where applicable:

- Accession codes, unique identifiers, or web links for publicly available datasets
- A description of any restrictions on data availability
- For clinical datasets or third party data, please ensure that the statement adheres to our policy

All data analyzed in this study are available in the manuscript and Extended

Data. The number of molecules included and the parameters for the raw survival curve fit for each replicate, uncorrected for framerate and labeling efficiency, are available in Supplemental Table 1. The large, raw movie files are available upon request to R.L.G.

Research involving human participants, their data, or biological material

Policy information about studies with human participants or human data. See also policy information about sex, gender (identity/presentation), and sexual orientation and race, ethnicity and racism.

Reporting on sex and gender	N/A
Reporting on race, ethnicity, or other socially relevant groupings	N/A
Population characteristics	N/A
Recruitment	N/A
Ethics oversight	N/A

Note that full information on the approval of the study protocol must also be provided in the manuscript.

Field-specific reporting

Please select the one below that is the best fit for your research. If you are not sure, read the appropriate sections before making your selection.

☒ Life sciences ☐ Behavioural & social sciences ☐ Ecological, evolutionary & environmental sciences

For a reference copy of the document with all sections, see nature.com/documents/nr-reporting-summary-flat.pdf

Life sciences study design

All studies must disclose on these points even when the disclosure is negative.

Sample size	No statistical methods were used to determine sample size. Trace counts of approximately 100 molecules are sufficient to accurately determine rates. Therefore, every single-molecule experiment was performed in biological duplicate to verify reproducibility and each replicate contained a sufficient (~>100) single molecule trajectories upon which survival analysis was performed. Two experiments, ejection of Cy5-eIF4G:E from the internal mRNA with and without eIF4A and ATP, contained a low number of trajectories and were repeated an additional time. The ejection experiments with the second internal labeling position rpl41a A211 was repeated four times due to low trace counts.
Data exclusions	Trajectories were filtered for signal-to-noise ratio and the characteristics of a single-molecule (single-step photobleaching or photoblinking). All single-molecule trajectories with a signal-to-noise ratio >5 were included in the analysis.
Replication	All single-molecule experiments were performed in biological duplicate. Additionally, many experiments were performed where the fluorophore was moved to another protein in the complex (Cy5-eIF4G:E vs eIF4G:E-Cy5). The titration-regime anisotropy experiments were performed once each, but with two different concentrations of RNA in the titration-regime. All attempts at replication were successful.
Randomization	For the type of quantitative, biochemical experiments performed in this article assignment of groups is not necessary for accurate analysis of the data. Therefore no group randomization was performed.
Blinding	For the type of quantitative, biochemical experiments peformed in this article, no group assignment is performed and consequently, blinding the experimenter to the group is not necessary.

Reporting for specific materials, systems and methods

We require information from authors about some types of materials, experimental systems and methods used in many studies. Here, indicate whether each material, system or method listed is relevant to your study. If you are not sure if a list item applies to your research, read the appropriate section before selecting a response.

Materials & experimental systems

n/a	Involved in the study
☒	☐ Antibodies
☒	☐ Eukaryotic cell lines
☒	☐ Palaeontology and archaeology
☒	☐ Animals and other organisms
☒	☐ Clinical data
☒	☐ Dual use research of concern
☒	☐ Plants

Methods

n/a	Involved in the study
☒	☐ ChIP-seq
☒	☐ Flow cytometry
☒	☐ MRI-based neuroimaging

Plants

Seed stocks	N/A
Novel plant genotypes	N/A
Authentication	N/A